Lithos 126 (2011) 84–98

Contents lists available at ScienceDirect

Lithos

journal homepage: www.elsevier.com/locate/lithos

Zircon dating, Hf–Sr–Nd–Os isotopes and PGE geochemistry of the Tianyu sulfide-bearing mafic–ultramafic intrusion in the Central Asian Orogenic Belt, NW China

Dongmei Tang [a,*], Kezhang Qin [a], Chusi Li [b,*], Liang Qi [c], Benxun Su [a], Wenjun Qu [d]

[a] Key Laboratory of Mineral Resources, Institute of Geology and Geophysics, Chinese Academy of Sciences, Beijing 100029, China
[b] Department of Geological Sciences, Indiana University, Bloomington, IN 47405, USA
[c] Institute of Geochemistry of Chinese Academy of Sciences, Guiyang, 550002, China
[d] National Research Center of Geoanalysis, Chinese Academy of Geological Sciences, Beijing, 100037, China

ARTICLE INFO

Article history:
Received 28 December 2010
Accepted 20 June 2011
Available online 1 July 2011

Keywords:
Slab break-off
Asthenosphere upwelling
Mafic–ultramafic rocks
Magmatic Ni–Cu deposit
Tianyu intrusion
Central Asian Orogenic Belt, China

ABSTRACT

The Tianyu mafic–ultramafic intrusion is one of many important sulfide-bearing mafic–ultramafic intrusions in the eastern Tianshan terrane located in the southern margin of the Central Asian Orogenic Belt in north Xinjiang, NW China. The origin of sulfide mineralization in these intrusions, their relationship with Permian basalts and A-type granites, and the geodynamic setting of the bimodal magmatism in the region are controversial. In this paper we use zircon U–Pb age, Hf–Sr–Nd–Os isotope and lithophile–chalcophile trace element constraints from the Tianyu mafic–ultramafic intrusion to address these important issues. The U–Pb age of zircon from the Tianyu intrusion determined by SIMS is 280 ± 2 Ma. This confirms that the Tianyu intrusion is coeval with most sulfide-bearing mafic–ultramafic intrusions and some basalts and A-type granites in the Tianshan region. Similar to coeval basalts in the nearby Tuha basin, the Tianyu intrusive rocks are characterized by negative Nb anomaly and elevated ε_{Nd} values varying between −1 and +4.6. The negative Nb anomaly in the Tianyu intrusion is not as pronounced as in the coeval A-type granites but the ε_{Nd} values for these bimodal rocks are similar. The ε_{Hf} values of zircon from the Tianyu intrusion are positive, varying between 3 and 8. These values suggest that the parental magma of the Tianyu intrusion was dominated by melt derived from a depleted source mantle. The γ_{Os} values of pyrrhotite from the Tianyu intrusion are high, ranging from 725 to 995, which can be modeled by selective assimilation of sulfide from the lower and upper crusts. Negative Pt anomaly is present in relatively sulfide-rich samples such as semi-massive and massive sulfide ores but not in sulfide-poor samples, which is more consistent with the effect of post-magmatic hydrothermal alteration than the original signature of the parental magma. The results of modeling using the compositions of selected disseminated sulfide samples suggest that the parental magma of the Tianyu intrusion was depleted in all PGE, which is consistent with previous sulfide segregation at depth. Our data and modeling results support the model of decompression melting of upwelling asthenosphere due to slab break-off during a transition from oceanic subduction to arc–arc or arc–continent collision in the Permian. Decompression melting of the upwelling asthenosphere in the region produced mafic magma. Partial melting in the lower parts of a juvenile arc crust due to mafic magma underplating produced granitic melts. Mixing of the mafic magma with a small amount of granitic melts at depth followed by contamination with the upper crust at a higher level formed the parental magma of the Tianyu intrusion. PGE depletion in the parental magma of the Tianyu intrusion can be attributed to sulfide segregation associated to the first stage of crustal contamination at depth. We suggest that the formation of sulfide ores in the intrusion was related to the second stage of crustal contamination in the upper crust.

1. Introduction

The Permian is an important period of continental basaltic magmatism in the world, producing voluminous flood basalts in Siberia, Russia and Emeishan, SW China (Fig. 1). Recently, another Permian flood basalt province was discovered in the Tarim basin by drilling for oil and gas (Chen et al., 1997). The Tarim basin is located in the western part of the Tarim Craton (Fig. 1). Ar–Ar dating of the flood basalts reveals the eruption ages varying from 262 to 285 Ma (Zhang et al., 2010a). The zircon U–Pb ages of rhyolite interbedded within the basalt sequence vary between 291 and 272 Ma (Tian et al., 2010). Mafic intrusions in the western rim of the basin, thought to be co-magmatic with the flood basalts, yield zircon U–Pb ages of ~275 Ma (Zhang et al., 2010b). Most recently, Permian basalts were also found in several locations north of

* Corresponding authors. Tel.: +86 1082998190; fax: +86 10 62010846.
E-mail addresses: tdm@mail.iggcas.ac.cn (D. Tang), cli@indiana.edu (C. Li).

0024-4937/$ – see front matter © 2011 Elsevier B.V. All rights reserved.
doi:10.1016/j.lithos.2011.06.007

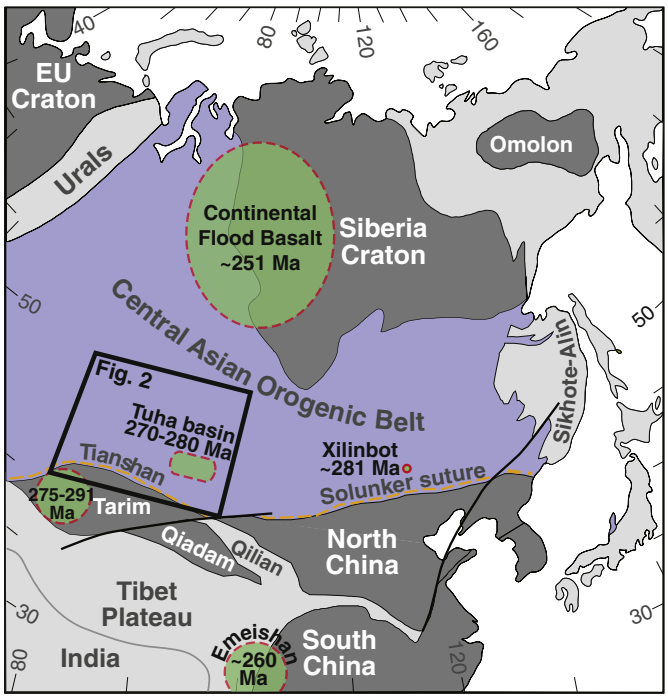

Fig. 1. Permian basaltic magmatism in Asia, modified from Li et al. (2011). The tectonic units are based on Jahn (2004) and Xiao et al. (2009b). The ages of basaltic magmatism are from Fan et al. (2008) for Emeishan basalts, Kamo et al. (2003) for Siberian basalts, Zhang et al. (2010) for Tarim basalts; Zhou et al. (2006) for Tuha basalts and Zhang et al. (2008) for Xilinbot basalts.

the Tarim Craton and within the Chinese part of the Central Asian Orogenic Belt (CAOB) (Fig. 1). Ar–Ar dating reveals that the Tuha basalts were erupted between 266 and 293 Ma (Zhou et al., 2006). The zircon U–Pb age of the Permian volcanic rocks in the Xilinbot region, NE China is ~281 Ma (Zhang et al., 2008). Numerous small mafic–ultramafic intrusions of Permian ages occur as clusters at several locations in northern Xinjiang. These intrusions have attracted a lot of attention lately because some of them such as the Huangshandong, Huangshanxi and Tianyu intrusions host economic sulfide mineralization (Fig. 2). The geodynamic settings of these intrusions, their relation to coeval basalts of contrasting compositions in the Tuha and Tarim basins, and the origin of sulfide mineralization in the intrusions are controversial. In this paper we use zircon U–Pb age, and integrated petrological, elemental and isotopic constraints from the Tianyu sulfide-bearing mafic–ultramafic intrusion to address these important issues.

2. Geological background

The Central Asian Orogenic Belt (CAOB) is the largest Phanerozoic juvenile orogenic belt in the world, extending 7000 km from west to east and from the Siberian Craton in the north to the Tarim Craton in the south (Fig. 1, Jahn et al., 2000, 2004; Sengör et al., 1993; Windley et al., 2007; Wong et al., 2010; Xiao et al., 2009a). With respect to crustal growth, magmatism and metallogeny, Late Paleozoic is the most important period for the CAOB in Xinjiang, China (Qin et al., 2003; Xiao et al., 2009b; Zhang et al., 2010c).

The Chinese Tianshan orogenic belt is located in the southern part of the CAOB (Fig. 2, Gao et al., 1995, 2009; Hu et al., 2000; Jahn et al., 2000, 2004; Wong et al., 2010; Xiao et al., 2003; Zhang et al., 2002). Numerous A-type granite plutons of Paleozic ages are found at different locations in this region (Gu et al., 1990, 2006; Han et al., 1997; Wang et al., 2009; Zhu et al., 2006). The eastern part of the Chinese Tianshan is referred to as the

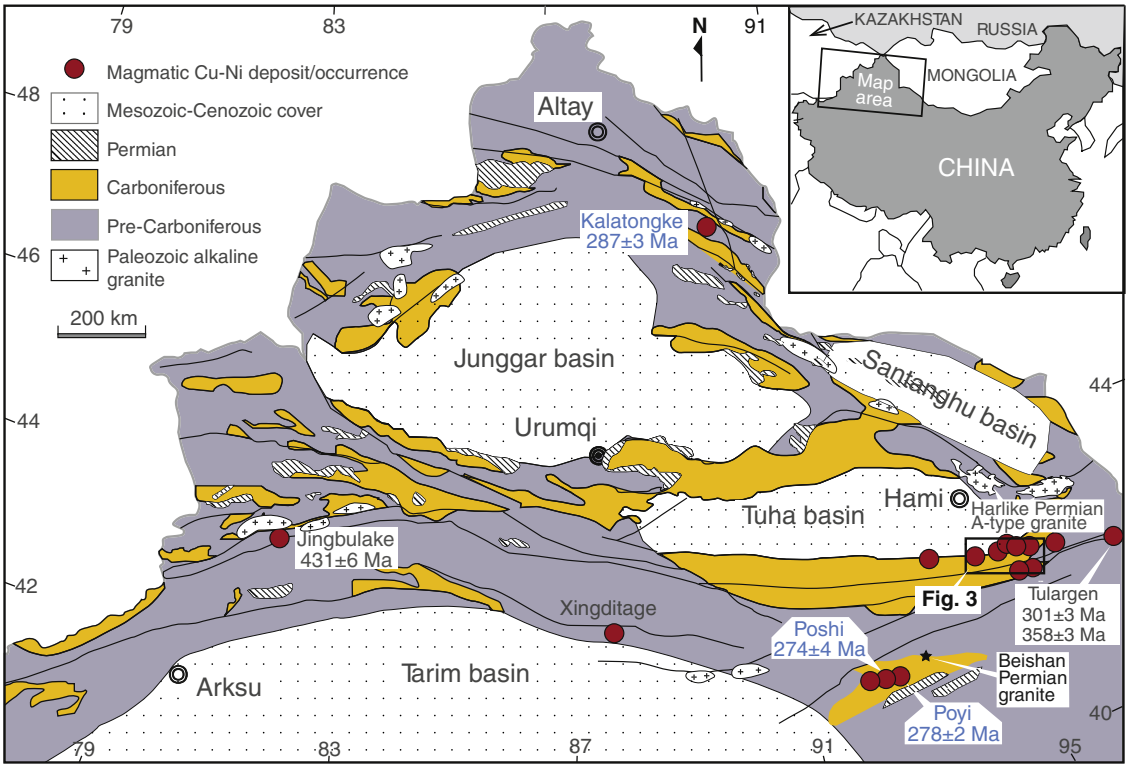

Fig. 2. Distribution of Cu–Ni deposits/occurrences associated with mafic–ultramafic intrusions in northern Xinjiang, modified from Zhang et al. (2010d). Sources of zircon U–Pb ages are from Yang and Zhou (2009) for the Jingbulake intrusion, Han et al. (2004) for the Kalatongke intrusion, Jiang et al. (2006) for the Poshi intrusion, Li et al. (2006) for the Poyi intrusion and San et al. (2010) for several mafic–ultramafic intrusion in the Tulargen area. Han et al. (1997), Su et al. (2011), Wang et al. (2009) and Zhu et al. (2006)for alkaline granite and Beishan Permian granite.

Eastern Tianshan in literature. It can be further divided into two subterranes: the Jueluotage and Central Tianshan, separated by the Aqikekuduke–Shaquanzi regional fault (Fig. 3a). The history of the Eastern Tianshan orogenic belt remains controversial. Some researchers suggested that the Eastern Tianshan resulted from southward subduction of the Junggar Ocean along the Bogeda–Haerlike zone (Ma et al., 1993; Qin, 2000; Zhang et al., 2004). Others proposed a northward subduction instead (Li et al., 2003; Wang et al., 2006). Zhou et al. (2008) proposed a multiple-stage subduction model for the evolution of the Paleo-Asian Ocean from Silurian to Early Carboniferous. The end of oceanic subduction in the region is still debated, with views varying from Late Carboniferous (Li, 2004; Li et al., 2006a,b; Wang et al., 2006; Zhang et al., 2008) to Late Permian or Early Triassic (Ao et al., 2010; Xiao et al., 2009a, 2010). Those in favor of the former interpretation believe that the upper mantle in this region was modified by slab fluids due to previous oceanic subduction before Permian (Chai et al., 2008; Mao et al., 2008; Pirajno et al., 2008; Zhou et al., 2004).

3. Geology of the Tianyu intrusion

The Eastern Tianshan region, which is currently an important mining district in China (Hong et al., 2003; Mao et al., 2008; Qin et al., 2003; Zhang et al., 2008) has many mafic–ultramafic intrusions. Some of these intrusions including the Tianyu intrusion host magmatic Ni–Cu sulfide deposits (Fig. 3a). The Tianyu mafic–ultramafic intrusion is located in the northern margin of the Central Tianshan terrane. It is a dyke-like body with surface exposure of ~2000 m long and ~100 m wide (Fig. 3b). The vertical downward extension varies between 250 and 350 m (Fig. 3c). It intruded Precambrian metamorphic rocks with grades varying from greenschist to amphibolite (He et al., 1996) and

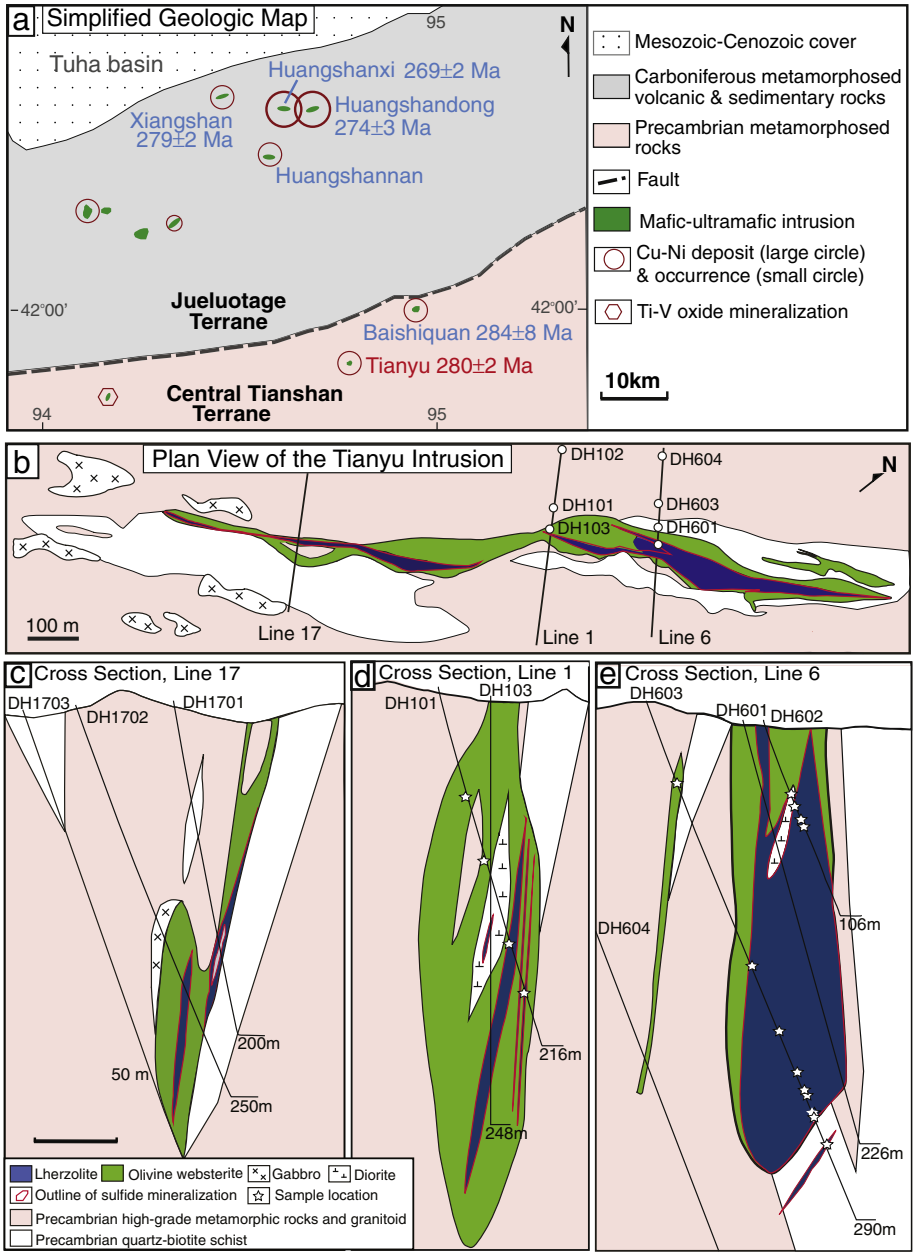

Fig. 3. (a) Simplified geologic map of Tianyu–Huangshan region. Not shown are Paleozoic granitoids. Sources of zircon U–Pb ages are from Wu et al. (2005) for the Baishiquan intrusion, Zhou et al. (2004) for the Huangshanxi intrusion, Han et al. (2004) for the Huangshandong intrusion, Xiao et al. (2010) for the Xiangshan intrusion and this study for the Tianyu intrusion. (b) and (c) are plan view and cross sections of the Tianyu intrusion, respectively.

Quaternary sedimentary rocks. Lherzolite, olivine websterite, gabbro and diorite are major rock units in the intrusion. The contacts between the ultramafic units and gabbro are gradational. The contact between diorite and the ultramafic rocks are sharp but no chilled margins between them are observed in the drill cores we have studied.

Lherzolite contains 50–70% olivine, 20–30% pyroxene plus minor (~3%) hornblende and phlogopite (~1%). Both clinopyroxene and orthopyroxene are present in the rock (Fig. 4a). Small Cr-spinel inclusions are present within some olivine crystals (Fig. 4b). Olivine websterite contains 20–30% olivine, 40–60% pyroxene, and 5–10% hornblende plus minor phlogopite. Olivine is anhedral to subhedral and commonly enclosed in large clinopyroxene (Fig. 4c) or orthopyroxene crystal (Fig. 4d). The forsterite contents of olivine in the ultramafic rocks vary between 78 and 85 mol%. Gabbro is characterized by the interlocking of randomly orientated tabular plagioclase and anhedral pyroxene (Fig. 4e). Minor hornblende, phlogopite and Fe–Ti oxides are also present in the rock. Diorite is characterized by a granular texture (Fig. 4f). In addition to plagioclase and pyroxene, hornblende and biotite are also abundant in diorite. The crystallization sequence inferred from the textures described above is olivine → pyroxene + plagioclase → hornblende + phlogopite. Minor Cr-spinel crystallized before and during olivine crystallization. Fe–Ti oxides crystallized with hornblende and phlogopite during the late stages. The inferred crystallization sequence is generally consistent with that of tholeiitic magma at shallow depths.

Similar to some other mafic–ultramafic intrusions in the region, the Tianyu intrusion contains economic sulfide mineralization. The sulfide

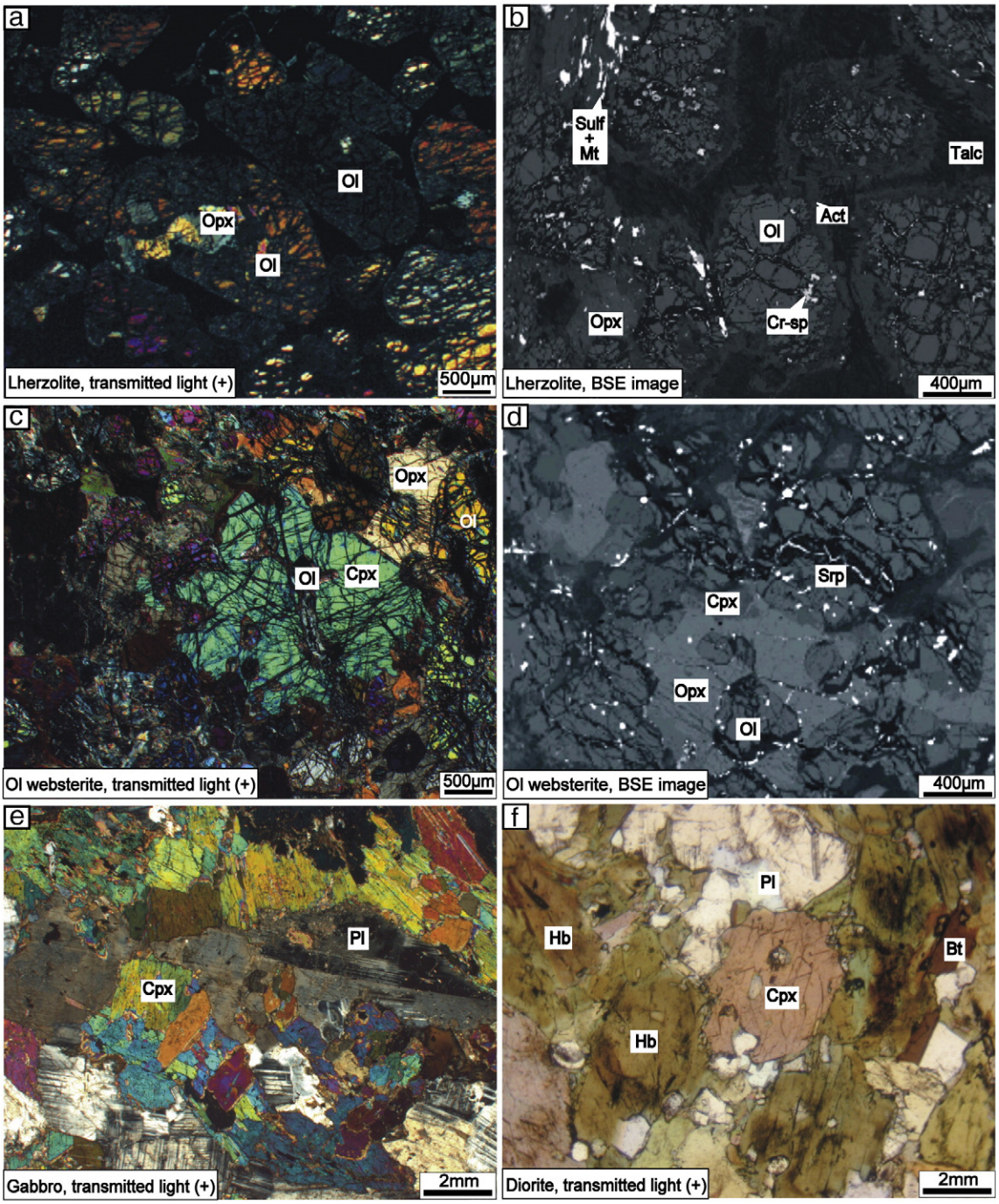

Fig. 4. Microphotographs and back-scattered electron (BSE) images showing the textures of important rock types in the Tianyu intrusion. Act = actinolite, Bt = biotite, Cr-spl = Cr-spinel, Cpx = clinopyroxene, Hb = hornblende, Mt = magnetite, Opx = orthopyroxene, Ol = olivine, Pl = plagioclase, Srp = serpentine, Sulf = sulfide.

mineralization occurs predominantly as disseminated and net-textured sulfides in the interstices of ultramafic rocks (Fig. 5a–b). Pyrrhotite, pentlandite and chalcopyrite are most important phases in the sulfide ores (Fig. 5c–d).

Hydrothermal alteration is ubiquitously present in the Tianyu intrusion. Olivine is partially altered to serpentine plus magnetite (Fig. 4a). Orthopyroxene is partially altered to talc and chlorite (Fig. 4b). Clinopyroxene is partially altered to actinolite or tremolite. Plagioclase is partially altered to sericite, epidote and albite. Secondary magnetite and pyrite are present in some sulfide mineralized samples.

4. Analytical methods

Whole rock major and trace elements were determined by XRF and by complete digestion of rock powders with HF + HNO_3 in Teflon bombs followed by ICP-MS analysis, respectively, at the Institute of Geology and Geophysics, Chinese Academy of Sciences in Beijing. The concentrations of PGE in sulfide mineralized samples were determined by the combination of NiS bead pre-concentration, Te co-precipitation and ICP-MS analysis in the National Research Center for Geo-Analysis, Beijing. The concentrations of PGE in sulfide-poor samples were determined by the Carius tube digestion and isotope dilution ICP-MS technique of Qi et al. (2007) at the Institute of Geochemistry, Chinese Academy of sciences in Guiyang. The detailed procedures of this technique, blank concentrations and detection limits are given in Qi et al. (2007).

SIMS (secondary ion mass spectrometry) zircon dating was conducted using a CAMECA IMS-1280 SIMS. The detailed analytical procedures were given in Li et al. (2009). Hf isotopes of zircon were determined using a multi-collector Thermo Electron Neptune MC-ICP-MS system. The detailed analytical procedures were given in Wu et al. (2006). The zircon dating and Hf isotopic measurement were conducted at the Institute of Geology and Geophysics, Chinese Academy of Sciences in Beijing.

Rb–Sr and Sm–Nd isotopes were determined using a Finnigan Mat 262 thermal ionization mass spectrometer at the Institute of Geology and Geophysics, Chinese Academy of Sciences in Beijing. The rock powders were treated with 0.3 N HCl for 1 h at ~100 °C, and dried after rinsing with purified water. The samples were weighed and spiked with mixed isotope tracers, dissolved in Teflon capsules with HF + HNO_3 at 120 °C for 7 days. Procedural blanks were <100 pg for Sm and Nd, and <500 pg for Rb and Sr. Mass fractionation corrections for Sr and Nd isotopic ratios were based on values of $^{86}Sr/^{88}Sr = 0.1194$ and $^{146}Nd/^{144}Nd = 0.7219$. Typical within-run precision (2σ) for Sr and Nd isotopic ratios is better than ±0.5% relative. The measured values for the LRIG Nd standard and the NBS987 Sr standard were $^{143}Nd/^{144}Nd = 0.512202 \pm 25$ and $^{87}Sr/^{86}Sr = 0.710245 \pm 35$ during the period of data acquisition.

Re–Os isotopes of sulfide minerals from the Tianyu deposit were obtained by isotope dilution ICP-MS (TJA PQ-EXCELL) and HR-ICP-MS methods in the National Research Center for Geo-Analysis, Beijing. The sulfide powders were loaded in a Carius tube through a thin neck long funnel. The ^{190}Os and ^{185}Re spike solutions from the Oak Ridge National Laboratory, USA, 2 mL of 12 M HCl and 6 mL of 15 M HNO_3 were loaded to the bottom of the tube at −50 to −80 °C. The top of the tube was sealed using an oxygen–propane torch. The tube was then placed in a stainless-steel jacket and heated for 10 h at 230 °C. Upon cooling, the bottom part of tube was kept frozen while the tube was broken at its neck. The contents of the tube were poured into a distillation flask and the residue was washed out of the tube with 40 mL pure water. Os was distilled two times. During the first time, OsO_4 was distilled at

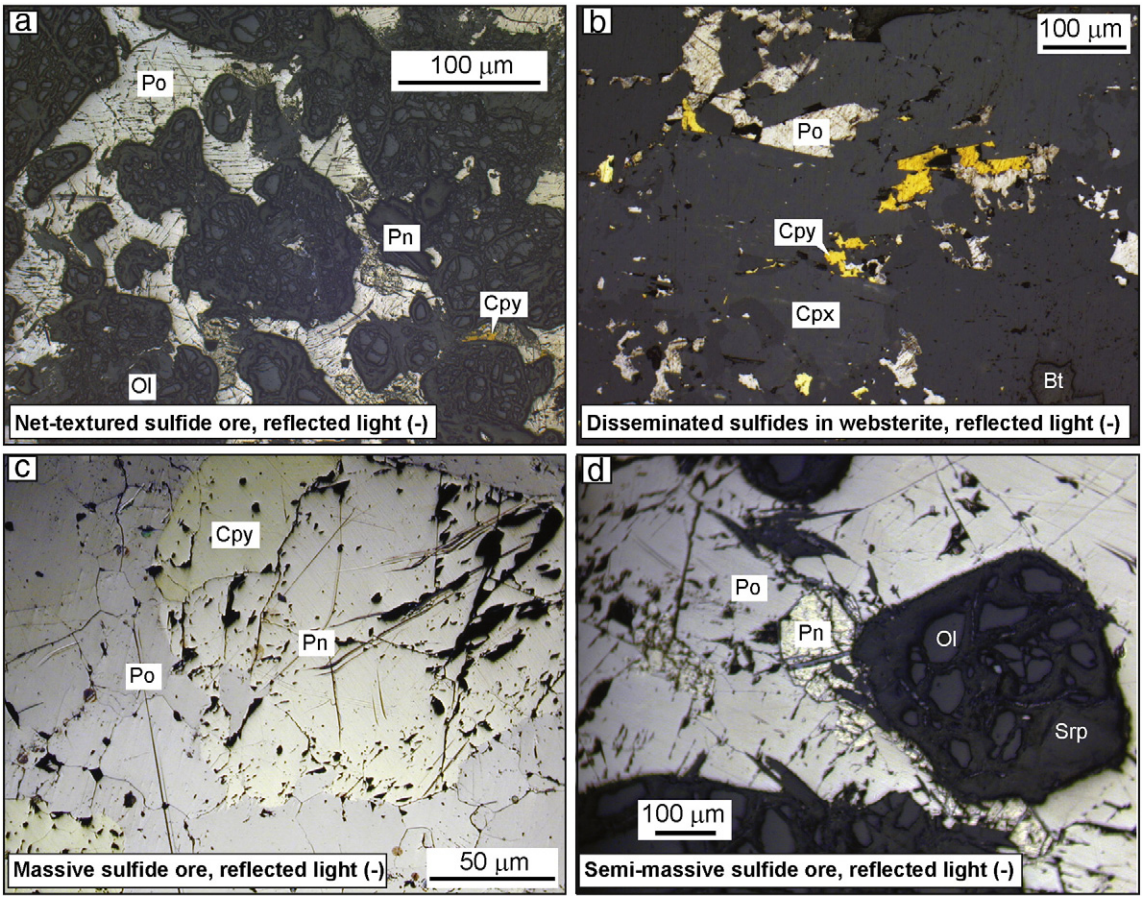

Fig. 5. Microphotographs showing the textures of net-textured sulfide (a), disseminated sulfide (b), massive sulfide (c) and semi-massive sulfide (d) ores in the Tianyu intrusion. Cpy = chalcopyrite, Pn = pentlandite, Po = pyrrhotite. Other mineral abbreviations are the same as in Fig. 4.

105 ~ 110 °C for 50 min and was collected in 10 mL pure water. The residual Re-bearing solution was saved in a 50 mL beaker for Re separation. The water trap solution plus 40 mL water were distilled a second time. The OsO_4 was distilled for 1 h and collected in 10 mL water for Os isotopic analysis by ICP-MS (TJA PQ-EXCELL). The Re-bearing solution was evaporated to dryness. 1 mL pure water was then added, and the solution was heated twice to dryness. 10 mL 20% NaOH was added to the residue. Re was then extracted using 10 mL acetone in a 120 mL Teflon separation funnel. 2 mL of 20% NaOH was added to the Re and transferred to a 100 mL beaker in which 2 mL water was present. The Re solution was evaporated to dryness, and the dissolved in 2% HNO_3 to form a final solution for Re isotopic analysis by HR-ICP-MS.

Sulfur contents in mafic–ultramafic rocks were determined using an automated LECO titration analytical system. The contents of sulfur in sulfide mineralized samples were determined by acid digestion followed by graphite-furnace AAS. The analyses were carried out at the Institute of Geology and Geophysics, Chinese Academy of Sciences, Beijing.

5. Results

5.1. Whole-rock major, trace and chalcophile elements

Whole-rock major and trace element compositions of the Tianyu intrusion are listed in Table 1. The ultramafic rock samples have relatively high and variable loss-on-ignition (LOI) values due to variable hydrothermal alteration. Variations of major oxide contents in the Tianyu rock samples normalized to 100% anhydrous composition are illustrated in Fig. 6a–f. The contents of MgO in lherzolite and olivine websterite samples overlap, but the former has lower SiO_2, CaO and Al_2O_3 (Fig. 6a,b,c). The contents of TiO_2 in the ultramafic rocks are <1 wt. % (Fig. 6d). Total iron oxide content (expressed as $Fe_2O_3^{Total}$) increases

Table 1
Whole rock major and trace element compositions of the Tianyu mafic–ultramafic intrusion.

Sample	T603–52	T602–49	T602–29	T602–58	T603–39	T101–72	T101–51	T204–202	T203–170	T803–64	T–12	1400-3	1450-3	1500-8	1500-6
Rock type	Diorite	Light colored gabbro	Olivine websterite								Lherzolite				
SiO_2	52.06	50.97	45.70	35.89	42.98	45.25	43.25	42.94	37.7	36.78	25.62	27.77	33.35	24.29	26.88
TiO_2	1.00	0.56	0.50	0.51	0.60	0.41	0.45	0.39	0.71	0.86	0.22	0.72	0.92	0.17	0.25
Al_2O_3	15.95	15.36	9.32	9.74	9.17	6.27	6.83	7.13	8.17	8.41	1.83	3.36	4.48	0.88	3.33
$Fe_2O_3^{Total}$	10.71	14.08	14.21	22.27	11.30	12.52	13.10	16.33	18.70	22.93	30.40	31.44	24.64	38.00	32.59
MnO	0.09	0.13	0.15	0.14	0.18	0.14	0.16	0.10	0.14	0.18	0.34	0.25	0.25	0.20	0.28
MgO	2.70	5.34	15.40	19.15	25.02	24.08	22.98	21.39	22.23	18.33	29.13	25.54	26.72	26.06	24.56
CaO	8.43	3.32	5.60	4.25	3.12	4.06	6.57	5.52	4.75	4.32	0.87	1.63	1.57	0.49	1.43
Na_2O	4.17	5.34	2.12	0.44	0.17	0.01	0.23	0.4	0.32	0.49	0.12	0.47	0.45	0.01	0.27
K_2O	2.13	0.88	1.97	0.09	1.51	0.03	0.10	0.57	0.06	1.00	0.04	0.20	0.35	0.05	0.08
P_2O_5	0.42	0.32	0.10	0.16	0.13	0.14	0.10	0.11	0.22	0.23	0.04	0.16	0.15	0.03	0.03
LOI	1.72	3.19	4.41	6.92	5.96	7.04	5.91	4.49	6.82	5.86	10.39	7.31	6.32	8.41	9.52
Total	99.38	99.49	99.48	99.56	100.14	99.95	99.68	99.37	99.82	99.39	99	98.85	99.2	98.58	99.22
Li	31.9	13.8	31.1	17.2	9.75	1.78	2.41	43.9	6.0	21.0	10.2	6.2	12.9	3.0	8.8
Be	2.6	1.7	0.7	0.6	0.5	0.3	0.5	0.9	0.8	1.0	1.4	1.4	1.2	1.1	0.9
Sc	12.4	7.4	19.5	12.0	13.4	14.5	20.2	7.8	13.4	14.3	5.6	9.4	15.9	5.3	9.6
V	106	31	108	82	90	77	86	61	103	117	38	76	101	37	71
Cr	9	170	1263	1384	514	1769	1676	1519	1768	1339	1440	1526	1705	757	587
Co	8	184	178	262	110	144	112	182	141	268	716	520	234	514	577
Ni	4	2152	2571	4558	377.9	1361	929.2	5342	1837	4507	5160	4561	2311	2708	4717
Cu	3	5453	410	627	91	314	335	2553	538	606	3008	3099	514	22,382	5454
Zn	72	104	88	111	94.3	115	95.4	245	88.8	110	140	166	145	233	192
Ga	24	13	11	10	9	7	7	12	9	9	3	6	7	2	4
Rb	118	34	69	2	101	1	8	68	1	41	4	9	18	2	4
Sr	358	1293	241	53	34	47	101	422	83	8	64	106	112	26	81
Y	44.9	13.6	11.0	9.4	11.1	7.3	10.0	7.1	13.0	12.1	2.3	7.9	11.2	2.5	3.3
Zr	375	873	55	74	77	54	45	53	111	81	10	67	44	23	26
Nb	13.3	5.7	3.2	3.4	3.3	2.4	2.2	2.5	5.0	4.8	0.6	2.7	3.6	0.3	0.4
Cs	11.4	2.2	11.5	1.2	14.7	1.2	2.2	5.9	1.1	6.2	1.4	0.9	4.0	0.2	0.6
Ba	376	1059	217	36	116	25	6	208	34	117	8	58	62	14	26
La	61.51	23.86	6.41	8.55	8.35	6.79	5.66	7.39	10.61	11.04	1.76	5.96	8.27	0.78	0.94
Ce	126.19	44.07	15.32	18.8	18.01	15.79	12.99	14.86	25.49	24.16	3.97	13.50	18.70	1.85	2.24
Pr	14.81	5.24	2.05	2.36	2.3	2.08	1.82	1.78	3.41	3.14	0.50	1.74	2.49	0.26	0.30
Nd	56.13	17.02	8.65	9.46	9.18	8.48	7.9	6.72	13.85	12.38	2.27	7.93	11.20	1.23	1.61
Sm	10.31	3.04	2.08	2.12	2.17	1.80	1.98	1.53	3.27	2.84	0.459	1.62	2.39	0.36	0.40
Eu	1.9	1.02	0.69	0.67	0.39	0.30	0.47	0.58	0.79	0.77	0.16	0.47	0.66	0.12	0.20
Gd	9.62	2.62	1.96	1.99	2.11	1.60	2.06	1.40	2.90	2.67	0.43	1.48	2.21	0.40	0.46
Tb	1.46	0.38	0.31	0.32	0.34	0.25	0.32	0.22	0.45	0.42	0.09	0.29	0.41	0.08	0.10
Dy	8.55	2.23	1.94	1.81	2.05	1.41	1.87	1.32	2.60	2.39	0.42	1.42	2.03	0.45	0.62
Ho	1.71	0.49	0.41	0.36	0.42	0.28	0.37	0.26	0.53	0.46	0.08	0.27	0.38	0.08	0.10
Er	4.62	1.44	1.08	0.95	1.18	0.73	0.99	0.70	1.41	1.19	0.28	0.79	1.24	0.24	0.36
Tm	0.65	0.25	0.16	0.14	0.18	0.11	0.15	0.10	0.20	0.17	0.04	0.12	0.19	0.04	0.04
Yb	4.09	1.82	1.04	0.92	1.13	0.65	0.94	0.61	1.23	1.02	0.23	0.75	1.06	0.25	0.37
Lu	0.61	0.32	0.16	0.13	0.17	0.10	0.14	0.09	0.18	0.15	0.03	0.11	0.13	0.04	0.05
Hf	9.8	23.5	1.5	1.7	1.9	1.3	1.3	1.2	2.5	2.0	0.2	1.2	1.1	0.4	0.5
Ta	1.05	0.64	0.23	0.26	0.22	0.18	0.14	0.18	0.35	0.36	0.07	0.19	0.23	0.03	0.03
Tl	0.62	0.14	0.63	0.07	0.79	0.15	0.21	0.52	0.09	0.37	0.03	0.11	0.29	0.07	0.13
Pb	23.1	34.3	5.1	4.9	1.8	4.9	3.2	44.6	4.3	4.8	18.0	33.1	9.3	32.3	38.5
Bi	0.12	2.49	0.63	1.80	0.44	1.27	0.65	1.59	1.21	1.50	4.53	3.74	1.37	2.04	2.71
Th	12.4	8.5	1.5	1.0	1.4	0.7	0.5	0.7	1.2	2.0	0.2	0.6	0.9	0.1	0.1
U	2.31	2.41	0.47	0.27	0.35	0.20	0.17	0.23	0.38	0.66	0.08	0.19	0.29	0.04	0.06

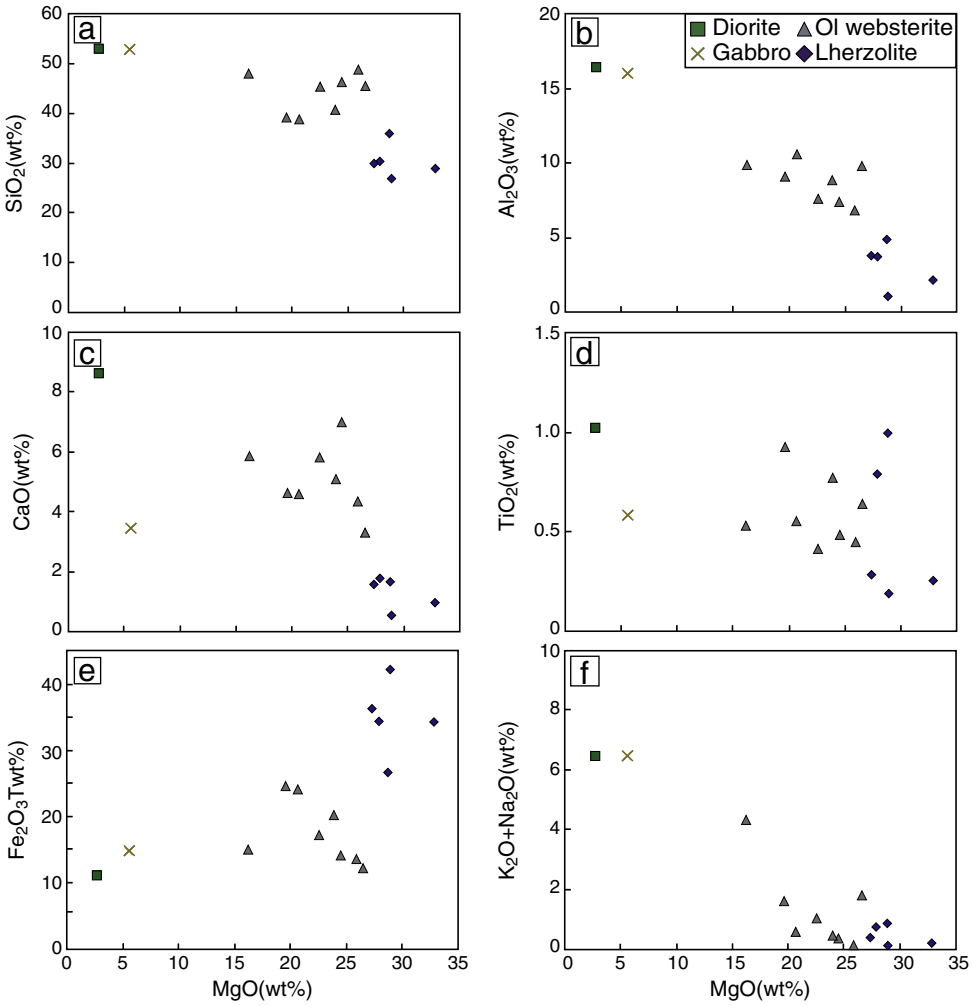

Fig. 6. Harker plots of whole rock compositions normalized to 100% oxides free of LOI for the Tianyu mafic–ultramafic intrusion.

with decreasing MgO content (Fig. 6e). Except one sample, all other ultramafic rock samples have total alkaline oxides <2 wt.%. The gabbro and diorite samples have much higher alkaline oxide concentrations (Fig. 6f).

The chondrite-normalized rare-earth element (REE) and primitive mantle-normalized alteration-resistant trace element patterns for the Tianyu intrusion are illustrated in Fig. 7a–b. Since these elements are incompatible during the crystallization of Cr-spinel and major silicate minerals, the abundances of these elements mainly reflect the degrees of fractionation as well as the amounts of "trapped liquid" prior to complete solidification of the rocks. The trace element patterns of different types of rocks in the Tianyu intrusion are sub-parallel, suggesting that the different rock types are related to each other by magma differentiation and crystal sorting. The Tianyu intrusive rocks and the Tarim basalts have similar trace element patterns except Nb and Ta. Pronounced negative Nb–Ta anomalies relative to Th and La which characterize the Tianyu intrusive rocks are not present in the Tarim basalts.

The concentrations of platinum-group elements (PGE), Cu, Ni, and S in the sulfide mineralized samples are listed in Table 2. The primitive mantle-normalized patterns of these elements in recalculated 100% sulfide compositions (referred to as tenors hereafter) are illustrated in Fig. 8a–c. The recalculated values more closely reflect the compositions of parental sulfide liquids than the whole rock data. In our recalculation Ni contribution from silicates (mainly from olivine) was corrected using the average content of Ni in sulfide-poor samples of respective rock types. Bulk sulfide contents in the samples were calculated using whole-rock S, Ni and Cu contents based on the average compositions of pyrrhotite, pentlandite and chalcopyrite and a common procedure given in a review by Barnes and Lightfoot (2005). As shown in Fig. 8a–c, samples with different sulfide abundances exhibit different chalcophile element patterns. The sulfide-poor samples don't have Pt anomaly relative to Rh and Pd (Fig. 8a). Most disseminated sulfide samples also don't have Pt anomaly, only 2 of them show either positive or negative Pt anomaly (Fig. 8b). The net-textured, semi-massive and massive sulfide samples we have analyzed all exhibit negative Pt anomaly (Fig. 8c).

5.2. Zircon U–Pb ages and Hf isotopes

The cathodoluminescence images of zircons from the Tianyu gabbros are illustrated in Fig. 9a. They are small, colorless, euhedral to subhedral crystals with sector zoning (Fig. 9a). Their U, Th and Pb contents, and U–Pb isotopes determined by in situ SIMS technique are listed in Table 3. Fig. 9b is a concordia plot for the data and the condordia age is 280 ± 2 Ma (95% confidence, MSWD = 0.92, n = 18).

The Hf isotopes of zircon crystals determined by in situ LA-MC-ICP-MS are listed in Table 4. The ε_{Hf} (t = 280 Ma) values of the Tianyu zircons vary between 3 and 8. These values are slightly lower that the values of zircons from the nearby Xiangshan mafic–ultramafic intrusion with similar age (see Figs. 3a and 10). Numerical modeling of crustal contamination using zircon Hf isotopes will be given below.

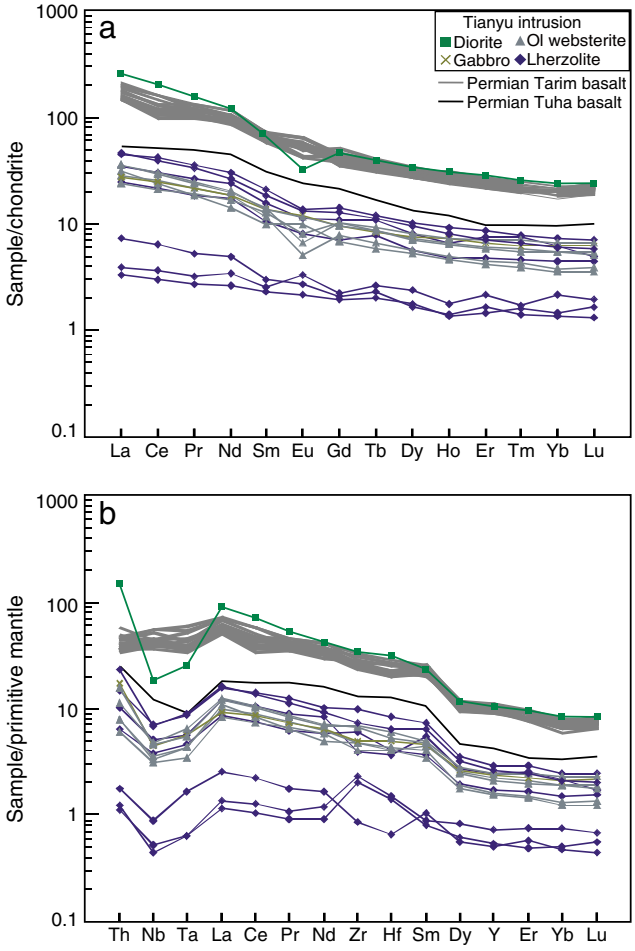

Fig. 7. Chondrite-normalized REE patterns (a) and primitive mantle-normalized alteration-resistant trace element patterns of Tianyu intrusive rocks and coeval basalts in the Tarim and Tuha basins. Data for the Tarim basalts are from Zhou et al. (2009). Data for the Tuha basalts are from Zhou et al. (2006). The chondrite values and the primitive mantle values are from Anders and Grevesse (1989) and Sun and McDonough (1989), respectively.

5.3. Rb–Sr and Sm–Nd isotopes

The Rb–Sr and Sm–Nd isotopes of whole rock samples from the Tianyu intrusion are listed in Table 5. The calculated ε_{Nd} and initial $^{87}Sr/^{86}Sr$ values (t = 280 Ma) of the Tianyu intrusive rocks vary between −1.1 and 4.6, and between 0.747 and 0.785, respectively. A comparison of Sr–Nd isotopes for several mafic–ultramafic intrusions with similar ages in the region and the Tarim basalts is illustrated in Fig. 11. Samples from the Tianyu intrusion are plotted between the coeval mafic–ultramafic intrusions in the Tianshan region and the Tarim basalts.

5.4. Re–Os isotopes

The concentrations of Re and Os and their isotopic compositions in pyrrhotite separated from the Tianyu sulfide mineralized samples are listed in Table 6. The γ_{Os} (t = 280 Ma) values are high, varying between 725 and 995. The Re–Os isochron ages not only have extremely large errors, but also are significantly different from the precise zircon U–Pb age for the intrusion. The discrepancy is most likely due to the effect of postmagmatic hydrothermal alteration on the Re–Os systematics.

6. Discussion

6.1. Origin of negative Pt anomaly

Clearly, the negative Pt anomaly in the Tianyu intrusion is related to sulfide abundance in the samples. All sulfide-rich samples such as net-textured, semi-massive and massive sulfide samples exhibit negative Pt anomaly (Fig. 8c). All sulfide-poor samples and most disseminated sulfide samples do not show Pt anomaly (Fig. 8a–b). Similar phenomenon has also been observed in the Jinchuan mafic–ultramafic intrusion which hosts one of the largest Ni–Cu–(PGE) deposit in the world. Song et al. (2009) suggested that negative Pt anomaly in the Jinchuan sulfide-rich samples reflects parental magma composition. If this is true, it should not be restricted to only sulfide-rich samples. We suggest that the selective Pt anomaly in the Tianyu intrusion is related to sulfide liquid fractionation as well as postmagmatic hydrothermal alteration. On cooling, a magmatic sulfide liquid starts to crystallize monosulfide solid solution (MSS) at temperature ~1090 °C in the crust. Pt and Pd are enriched in the fractionated liquid because they are incompatible in the MSS structure (Li et al., 1996). When pentlandite starts to exsolve from MSS or directly appears on the liquidus of a fractionated liquid, Pt and Pd will fractionate from each other because Pd is compatible in pentlandite but Pt is not. Platinum prefers to form discrete minerals such as arsenide and telluride. Since pentlandite is a major phase whereas discrete Pt phases only occur at trace levels in original magmatic sulfide assemblages, their responses to postmagmatic hydrothermal

Table 2
Concentrations of S, Ni, Cu and PGE in sulfide mineralized samples from the Tianyu mafic–ultramafic intrusion.

Sample	Host rock	Mineralization	S	Ni	Cu	Pt	Pd	Rh	Ru	Ir	Os
			wt%			ppb					
TY603-123	lherzolite	Sulfide-poor	0.70	0.06	0.20	0.75	0.98	0.09	0.16	0.11	0.13
TY603-39	Ol websterite	Sulfide-poor	0.28	0.05	0.01	7.43	11.32	0.21	0.13	0.12	n.a.
TY101-72	Ol websterite	Sulfide-poor	0.20	0.12	0.30	1.50	1.98	0.13	0.14	0.08	n.a.
TY101-51	Ol websterite	Sulfide-poor	0.40	0.12	0.40	1.24	1.81	0.06	0.12	0.05	n.a.
TY602-49	Gabbro	Disseminated sulfide	4.33	0.38	1.31	2.35	8.64	0.22	0.25	0.25	0.34
TY602-29	Ol websterite	Disseminated sulfide	1.55	0.34	0.50	3.27	2.35	0.31	0.32	0.21	n.a.
TY602-58	Ol websterite	Disseminated sulfide	5.44	0.60	0.80	196.00	6.92	0.45	0.82	0.65	1.74
TY603-190	Ol websterite	Disseminated sulfide	3.37	0.46	0.70	10.00	13.00	0.36	1.06	0.50	1.45
TY602-57	lherzolite	Disseminated sulfide	2.44	0.18	1.66	6.23	5.16	0.26	0.52	0.41	0.65
TY603-183	lherzolite	Disseminated sulfide	2.64	0.26	0.03	9.40	12.23	0.37	0.20	0.13	n.a.
TY803-64	lherzolite	Disseminated sulfide	5.64	0.60	0.70	0.46	5.44	0.55	0.72	0.44	n.a.
TY101-153	Ol websterite	Net-textured sulfide	9.54	1.40	0.26	0.41	18.19	0.54	1.03	0.60	n.a.
TY603-235	lherzolite	Net-textured sulfide	12.19	0.70	13.32	1.37	28.40	5.62	13.60	7.97	19.60
TY603-247	lherzolite	Semi-massive sulfide	19.20	1.74	7.90	0.78	49.60	4.98	8.24	5.73	12.50
TY603-171	lherzolite	Semi-massive sulfide	24.02	2.74	1.73	0.83	148.00	0.65	1.21	1.28	0.99
TY101-184	Ol websterite	Massive sulfide ores	28.61	2.78	0.27	0.58	8.24	11.28	24.92	12.34	n.a.

n.a. = not analyzed.

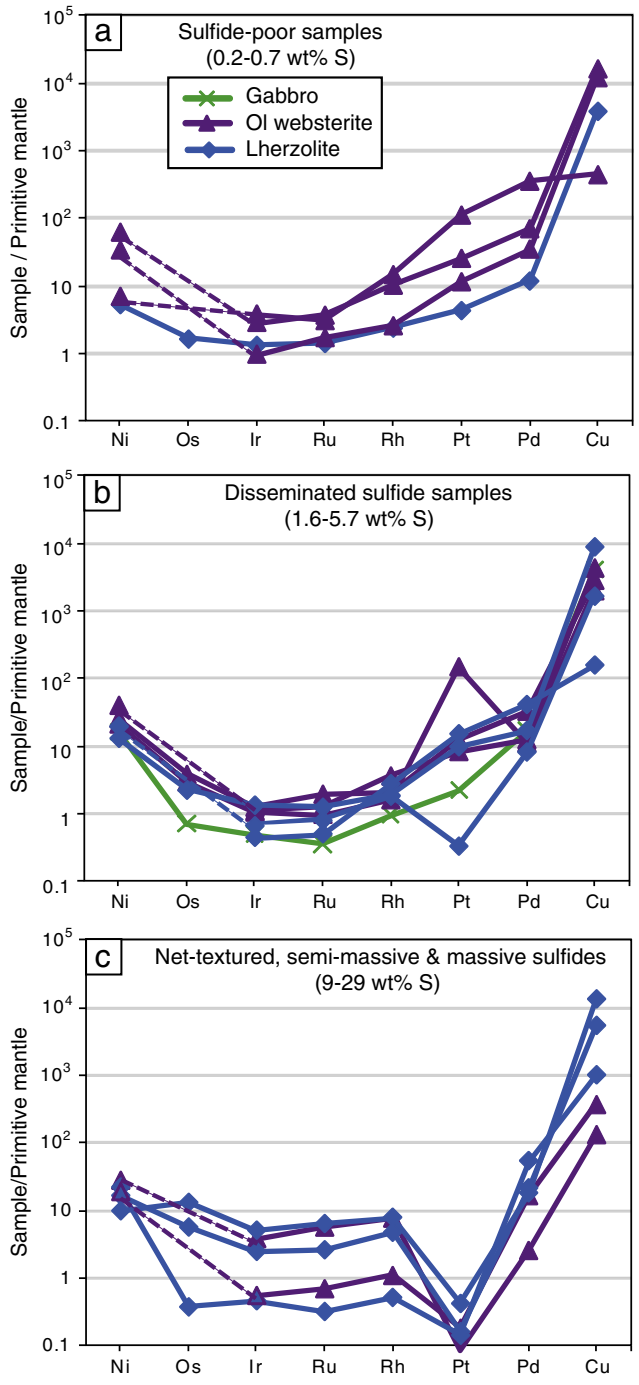

Fig. 8. Primitive mantle-normalized PGE patterns of the Huangshanxi deposit. The primitive mantle values are from Barnes and Maier (1999).

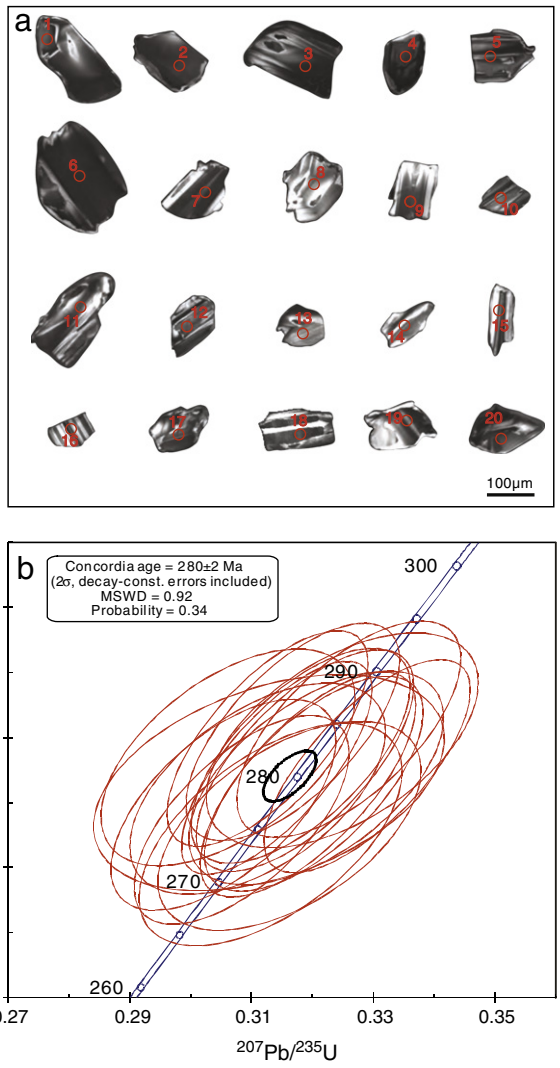

Fig. 9. Cathodoluminescence images of zircon (circles are targets of analysis) (a) and $^{207}Pb/^{235}U-^{206}Pb/^{238}U$ concordia diagram of zircon (b) from the Tianyu intrusion.

leaching can be dramatically different, thereby resulting in Pt and Pd decoupling at the sample scales. The tendency for negative Pt anomaly to occur in sulfide-rich samples suggests that these samples are more prone to hydrothermal alteration than the sulfide-poor samples. Higher degrees of serpentinization in the sulfide-rich samples (see Fig. 5a,d) than the sulfide-poor samples (see Fig. 4a–d) support such interpretation.

6.2. PGE depletion in parental magma

In magmatic sulfide deposits, PGE fractionation is more commonly observed in sulfide-rich samples such as net-textured, semi-massive and massive sulfide ores than in relatively sulfide poor samples. This is because fractionated sulfide liquid can escape more easily from sulfide-rich samples due to better connectivity of sulfide melt in the rocks (see a review by Barnes and Lightfoot, 2005). We have chosen the sulfide-poor samples and disseminated sulfide ores that do not have Pt anomaly to estimate PGE concentrations in the parental magma of the Tianyu intrusion. We assume that the PGE tenors in these samples represent original sulfide liquid composition and use the mass balance equation of Campbell and Naldrett (1979) for modeling. Our calculations indicate that variable R-factors between 200 and 1800 with initial contents of 0.01 ppb Ir, 0.02 ppb Os and 0.2 ppb Pd in the parental magma can explain the variations of metal tenors in these samples (Fig. 12a–b). The estimated concentrations of PGE in the Tianyu parental magma are almost one order of magnitude lower than their concentrations in the Permian PGE-undepleted basalts in Siberia (Lightfoot and Keays, 2005) and Emeishan (Qi and Zhou, 2008). The extent of PGE depletion in the Tianyu deposit is similar to some Ni–Cu sulfide deposits in the Emeishan large igneous province (e.g. Limahe and Baimazhai deposits, Song et al., 2008). There are two alternative explanations for PGE depletion in the parental magma of the Tianyu intrusion: (1) sulfide retention in the source mantle region or (2) previous sulfide segregation at depth. These will be discussed in more detail below.

Table 3
Concentrations of U, Th and Pb, and U–Pb isotopes of zircon from the Tianyu intrusion.

Sample	U (ppm)	Th (ppm)	Pb (ppm)	Th/U	$^{207}Pb/^{235}U$	±1σ (%)	$^{206}Pb/^{238}U$	±1σ (%)	$^{207}Pb/^{206}Pb$	±1σ (%)	$t_{206/238}$ (Ma)	±1σ (%)
TY-1	513	386	30	0.75	0.31882	2.29	0.0446	1.56	0.0526	1.51	281.6	4.3
TY-2	642	1012	44	1.58	0.31415	2.04	0.0445	1.50	0.0512	1.37	281.1	4.2
TY-3	427	471	26	1.10	0.30540	2.47	0.0440	1.51	0.0515	1.68	277.9	4.1
TY-4	552	74	27	0.13	0.32904	2.10	0.0446	1.50	0.0536	1.47	280.4	4.2
TY-5	500	556	31	1.11	0.31264	2.16	0.0450	1.50	0.0504	1.55	284.2	4.2
TY-6	718	981	48	1.37	0.32601	2.31	0.0451	1.50	0.0524	1.75	284.4	4.2
TY-7	428	672	30	1.57	0.31680	2.26	0.0451	1.51	0.0510	1.68	284.6	4.3
TY-8	105	99	6	0.94	0.31289	3.76	0.0443	1.53	0.0512	3.44	279.7	4.3
TY-9	400	600	27	1.50	0.31809	2.31	0.0447	1.51	0.0516	1.75	282.1	4.2
TY-10	302	46	15	0.15	0.32063	2.67	0.0444	1.51	0.0524	2.20	279.7	4.2
TY-11	558	701	35	1.26	0.31931	2.26	0.0443	1.60	0.0529	1.47	279.1	4.4
TY-12	395	59	19	0.15	0.30838	2.34	0.0437	1.50	0.0511	1.80	276.1	4.1
TY-13	429	82	21	0.19	0.31625	2.79	0.0436	1.50	0.0526	2.35	275.1	4.1
TY-14	437	49	21	0.11	0.31101	2.76	0.0442	1.50	0.0510	2.31	279.2	4.2
TY-15	486	602	31	1.24	0.32027	2.29	0.0443	1.52	0.0531	1.61	279.1	4.2
TY-16	261	259	16	0.99	0.32495	2.81	0.0450	1.50	0.0524	2.37	283.3	4.2
TY-17	565	795	36	1.41	0.31315	2.82	0.0435	1.61	0.0527	2.25	274.4	4.4
TY-18	306	51	15	0.17	0.30617	2.78	0.0447	1.52	0.0508	2.02	282.7	4.3

6.3. Source mantle characteristics and crustal contamination

As shown in Fig. 10, the positive ε_{Hf} values of zircon from the Tianyu intrusion are consistent with parental magma derived from a depleted source mantle followed by 10–15% crustal contamination. The Sr–Nd isotopes suggest a moderately depleted source mantle with ε_{Nd} ~4 for the parental magma plus up to 15% of crustal contamination (Fig. 13). As shown in Fig. 12, the average R-factor for the bulk sulfide ores of the Tianyu intrusion is ~400. The γ_{Os} values of pyrrhotite from the sulfide ores vary between 725 and 995 (Table 6), significantly higher than the mantle value (γ_{Os} ~0) but close to the value of sulfide minerals in the upper crust (γ_{Os} ~1250, Lambert et al., 1999). If sulfide saturation in the Tianyu magma is the result of selective assimilation of crustal sulfides, mass balance calculations using an R-factor of 400 suggest that contamination with both the lower crust (γ_{Os} ~6500, Lambert et al., 1999) and upper crust are possible.

The Sr–Nd isotopes of the Tianyu intrusions are consistent with mixing between a depleted mantle-derived melt and the upper crust (Fig. 11). However, the primitive mantle normalized Th/Nb ratios are not (Fig. 13). As shown in Fig. 7b, the abundance of Th in the Tianyu rock samples is positively correlated with that of other relatively more immobile trace elements such as REE. This suggests that the concentration of Th in the samples has not been significantly affected by postmagmatic hydrothermal alteration. Therefore, the variation of Th/Nb ratios in the Tianyu samples can be regarded as a primary signature. As shown in Fig. 13, many of the Tianyu samples are displaced to the right of the mantle–crust mixing line, similar to other coeval mafic–ultramafic intrusions in the Tianshan region. Such a regional anomaly may reflect the unusual composition of source mantle due to metasomatization by slab-derived fluids during previous subduction events (Zhang et al., 2010d; Zhou et al., 2004). Alternatively, it may have resulted from mixing with partial melts derived from the lower part of a juvenile arc crust during mafic magma underplating. Partial melting of juvenile arc crust due to mafic magma underplating is widely believed to be responsible for the formation of abundant A-type granites in the region that are characterized by positive ε_{Nd} and highly negative Nb anomaly (e.g., B.F. Han et al., 2010). To evaluate this possibility, we have used the composition of coeval A-type granites (Wang et al., 2009) in the nearby (see Fig. 2) Paleozoic Kalamaili–Harlik island arc (Gu et al., 1999; Ma et al., 1993) to represent a partial melt derived from a juvenile arc crust. The Kalamaili–Harlik granites are the best choice at present because no precise age and required geochemical data are available for those that occur more close to the Tianyu intrusion. We use a depleted mantle-derived melt to represent the primary magma of the Tianyu

Table 4
Hf isotopes of zircon from the 280 Ma Tianyu intrusion.

Sample ID	$^{176}Yb/^{177}Hf$	2σ	$^{176}Lu/^{177}Hf$	2σ	$^{176}Hf/^{177}Hf$	2σ	$^{176}Hf/^{177}Hfi$	ε_{Hf} (t)
TY-Hf-1	0.034632	0.000291	0.001182	0.000009	0.282725	0.000023	0.282719	4.3
TY-Hf-2	0.040698	0.000877	0.001383	0.000026	0.282773	0.000023	0.282766	5.9
TY-Hf-3	0.076652	0.000190	0.002515	0.000007	0.282740	0.000022	0.282727	4.6
TY-Hf-4	0.020661	0.000059	0.000850	0.000003	0.282699	0.000020	0.282695	3.4
TY-Hf-5	0.067362	0.000616	0.002299	0.000018	0.282776	0.000023	0.282764	5.9
TY-Hf-6	0.081010	0.000750	0.002665	0.000030	0.282759	0.000023	0.282745	5.2
TY-Hf-7	0.043408	0.000141	0.001555	0.000005	0.282774	0.000024	0.282766	5.9
TY-Hf-8	0.036566	0.000083	0.001341	0.000002	0.282737	0.000021	0.282730	4.7
TY-Hf-9	0.010894	0.000044	0.000484	0.000002	0.282739	0.000018	0.282736	4.9
TY-Hf-10	0.042761	0.002487	0.001506	0.000083	0.282760	0.000024	0.282752	5.4
TY-Hf-11	0.066191	0.000519	0.002407	0.000021	0.282784	0.000024	0.282772	6.1
TY-Hf-12	0.060972	0.000336	0.002043	0.000010	0.282688	0.000026	0.282677	2.8
TY-Hf-13	0.026972	0.000325	0.000991	0.000013	0.282775	0.000024	0.282770	6.1
TY-Hf-14	0.017776	0.000042	0.000860	0.000002	0.282766	0.000021	0.282762	5.8
TY-Hf-15	0.024713	0.000083	0.001082	0.000003	0.282718	0.000020	0.282713	4.1
TY-Hf-16	0.027848	0.000258	0.001107	0.000010	0.282712	0.000023	0.282706	3.8
TY-Hf-17	0.054048	0.000327	0.002111	0.000012	0.282765	0.000028	0.282754	5.5
TY-Hf-18	0.061471	0.000404	0.002306	0.000016	0.282714	0.000024	0.282702	3.7
TY-Hf-19	0.029675	0.000153	0.001169	0.000006	0.282820	0.000025	0.282814	7.6
TY-Hf-20	0.014060	0.000075	0.000664	0.000004	0.282704	0.000027	0.282700	3.6

ε_{Hf} calculated as defined by Blichert and Albarede (1997), ^{176}Lu decay constant $\lambda = 1.865 \times 10^{-11}$/year (Soderlund et al., 2004), t = 280 Ma.

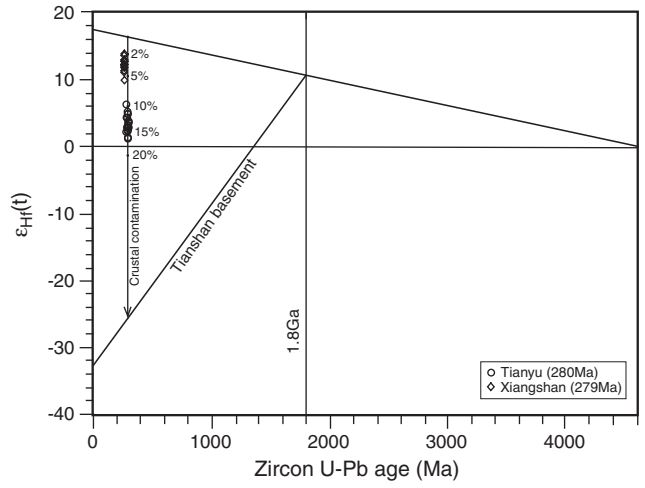

Fig. 10. Plot of ε_{Hf} versus U–Pb age of zircon from the Tianyu intrusion. The age of the Tianshan basement is based on Hu et al. (2000). The concentration of Hf in N-type MORB from Sun and McDonough (1989) is used to represent the composition of melt derived from depleted mantle. The evolution of Hf isotopes in the Tianshan basement is calculated using the parameters for the upper crust from Amelin et al. (1999). Hf isotopic data for the Xiangshan intrusion are from C.M. Han et al. (2010).

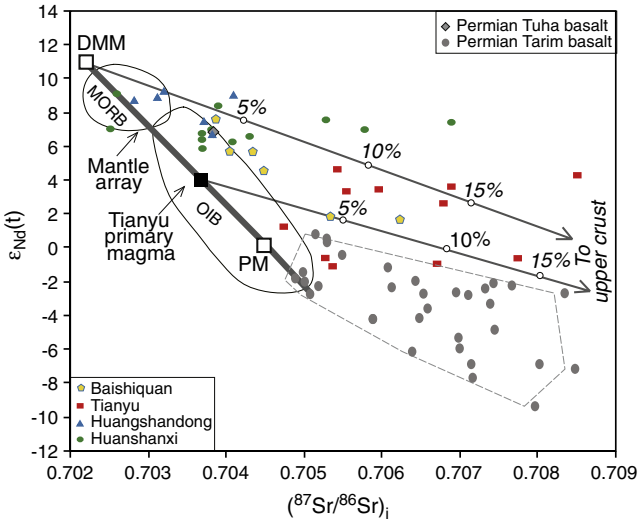

Fig. 11. Plot of ε_{Nd} (t) versus $(^{87}Sr/^{86}Sr)_i$ for several mafic–ultramafic intrusion in the Tianyu–Huangshan region the coeval basalts from the Tuha and Tarim basins. Data for the Tarim basalts are from Tian et al. (2010), Zhang et al. (2010) and Zhou et al. (2009). Data for the Tuha basalts are from Xia et al. (2008). Data for the Baishiquan intrusion are from Chai et al. (2008). Data for the Huangshandong intrusion are from Zhou et al. (2004). Data for the Huangshanxi intrusion are from Zhang et al. (2010d). Data for the Tianyu intrusion are from this study. Components for mixing calculations: depleted mantle-derived melt (DMM) (Zindler and Hart, 1986), 90 ppm Sr, 7.3 ppm Nd, $(^{87}Sr/^{86}Sr)_i = 0.7022$, ε_{Nd} (280 Ma) = 10.96; Upper crust (UC) (Rudnick and Gao, 2003), 320 ppm Sr, 27 ppm Nd, $(^{87}Sr/^{86}Sr)_i = 0.715$, ε_{Nd} (280 Ma) = −10. The proposed primary magma for the Tianyu intrusion has Sr and Nd contents the same as the DMM, ε_{Nd} (280 Ma) = 4 and $(^{87}Sr/^{86}Sr)_i = 0.7037$.

intrusion in our mixing calculations. Primary magma is defined as a mantle-derived melt prior to any crustal contamination and/or fractional crystallization. The results of our mixing calculations show that <10% contamination with the partial melt of the lower arc crust at depth followed by <10% contamination with the upper crust can well explain the variations of Nd isotopes and Th/Nb ratios in the Tianyu intrusion (Fig. 13). In our mixing calculations, the trace element concentrations and Nd isotopes for the granitic melt are taken from two different samples of the same pluton analyzed by Wang et al. (2009). The trace element data are based on sample X-387. This sample is most suitable to represent a granitic melt composition because it has very high incompatible trace element contents. However, since no Nd isotopic data are available for this sample, we used ε_{Nd} value of sample X-604 which has much lower trace element contents to represent the Nd isotopic composition of the granitic melt.

6.4. Assessment of competing geodynamic models

Various geodynamic models have been proposed for the Permian mafic–ultramafic intrusions in the Chinese part of the CAOB. Among them the mantle plume model has become very popular lately. This model was originally proposed by Zhou et al. (2004) based on their geochemical data for two Permian mafic–ultramafic intrusions in the Tianshan region. Recently, it has been extended to include the Permian alkaline basalts in the Tarim Craton by other researchers (Zhang et al., 2010b; Zhou et al., 2009). Zhang et al. (2010c) have suggested that the Permian mafic intrusions in the Chinese Altay such as the Kalatongke intrusion also belong to the same mantle plume. Su et al. (2011) suggested that the Permian mafic–ultramafic intrusions in the Beishan area (see Fig. 2) are part of the Tarim mantle plume. Qin et al. (2011) suggested that the Permian mafic–ultramafic intrusions in the Tianshan–Beishan region were produced by magma from the center of a mantle plume and the coeval alkaline basalts in the Tarim basin formed by melts from the peripheral part of the plume. If age is considered as the only constraint, one may also extend the Tarim mantle plume to include the Xilinbot basalts which occur several thousand km to the east (see Fig. 2). In fact, some researchers (Pirajno et al., 2008) have already suggested that the Emeishan, Tarim and Siberia flood basalt provinces that are temporally up to ~40 Ma difference and geographically up to 10,000 km apart (see Fig. 1) belong to a single mantle super plume. Obviously, it is difficult to assess the validity of any of the above plume models because our current knowledge about the duration, scale and source compositional variation of a single plume is very limited.

The second model for the Permian mafic–ultramafic intrusions in the CAOB is subduction-related magmatism (Xiao et al., 2004). In this model the Permian mafic–ultramafic intrusions including the Tianyu

Table 5
Sr–Nd data of whole rock samples from the 280 Ma Tianyu mafic–ultramafic intrusion.

Sample ID	Rock Type	Sm (ppm)	Nd (ppm)	$^{147}Sm/^{144}Nd$	$^{143}Nd/^{144}Nd$	ε_{Nd}	Rb (ppm)	Sr (ppm)	$^{87}Rb/^{86}Sr$	$^{87}Sr/^{86}Sr$	$(^{87}Sr/^{86}Sr)_i$
TY603-52	Diorite	9.74	51.52	0.11432	0.512458	−0.6	66.02	561.04	0.340543	0.706622	0.705265
TY602-49	Gabbor	2.77	16.74	0.100152	0.512417	−0.9	33.41	1771.71	0.054578	0.706945	0.706728
TY602-102	Gabbro	2.75	18.07	0.092173	0.512667	4.3	126.88	369.81	0.993553	0.712479	0.708521
TY602-29	Ol websterite	1.95	7.83	0.150575	0.512495	−1.1	68.95	240.94	0.828049	0.708677	0.705378
TY603-39	Ol websterite	1.56	5.39	0.175069	0.512731	2.6	100.59	30.77	0.94904	0.710586	0.706805
TY101-72	Ol websterite	1.31	5.37	0.147734	0.512735	3.6	1.77	47.75	0.107424	0.707338	0.706910
TY604-183	Ol websterite	2.29	7.87	0.176183	0.512777	3.4	26.2	59.89	0.866595	0.709424	0.705972
TY101-51	Lherzolite	1.94	6.89	0.170065	0.512757	3.3	18	103.72	0.502298	0.707563	0.705562
TY803-64	Lherzolite	2.51	9.34	0.16233	0.512635	1.2	40.59	84.23	1.394537	0.710303	0.704747
TY603-180	Lherzolite	0.72	3.22	0.135909	0.512764	4.6	6.33	161.64	0.113253	0.705887	0.705436

Values of $(^{87}Sr/^{86}Sr)_i$ and ε_{Nd} were calculated relative to present-day chondrite values of $^{143}Nd/^{144}Nd = 0.512638$, $^{147}Sm/^{144}Nd = 0.1967$, $^{87}Sr/^{86}Sr = 0.7045$ and $^{87}Rb/^{86}Sr = 0.0816$, $\lambda\ (^{87}Rb) = 1.42 \times 10^{-11}\ y^{-1}$, $\lambda\ (^{147}Sm) = 6.54 \times 10^{-12}\ y^{-1}$.

Table 6
Re–Os data of pyrrhotite separates from the 280 Ma Tianyu intrusion.

Sample	Re, ppb (2σ)	Os, ppb (2σ)	Re/Os	$^{187}Re/^{188}Os$ (2σ)	$^{187}Os/^{188}Os$ (2σ)	γ_{Os}
TY-7	134.60 (1.50)	11.16 (0.10)	12.06	58.27 (0.83)	1.426 (0.010)	814
TY-9	76.50 (0.62)	10.18 (0.10)	7.51	36.31 (0.48)	1.328 (0.013)	821
TY-4	38.11 (0.33)	3.94 (0.04)	9.67	46.71 (0.58)	1.596 (0.013)	995
TY-1	140.20 (1.60)	21.08 (0.21)	6.65	32.13 (0.49)	1.188 (0.011)	725
TY-6	141.90 (1.20)	9.45 (0.07)	15.01	72.47 (0.84)	1.657 (0.009)	943
TY-2	132.10 (1.00)	12.38 (0.11)	10.67	51.55 (0.60)	1.437 (0.011)	849
TY-3	121.20 (1.00)	12.23 (0.10)	9.91	47.85 (0.56)	1.437 (0.009)	863
TY-10	76.24 (0.67)	0.21 (0.0018)	367.78	1776 (22)	9.821 (0.066)	851

γ_{Os} calculated as defined by Shirey and Walker (1998).

intrusion are regarded as typical Alaskan-type zoned complexes. Data from Li et al. (2011), Zhang et al. (2010d) and Zhou et al. (2004) indicate that they are tholeiitic intrusions rather than typical Alaskan-type calc–alkaline complexes. Nevertheless, this does not completely rule out the subduction zone model because in addition to dominant calc–alkaline magma, minor tholeiitic magma may also be produced by subduction zone magmatism (e.g., Pearce et al., 1995). However, the results of available studies indicate that the Permian mafic–ultramafic intrusions in the Tianshan region are all tholeiitic intrusions (Zhang et al., 2010d; Zhou et al., 2004). Many of them also contain important sulfide mineralization. Calc–alkaline magma produced by flush melting in the mantle wedge may be too oxidized to form magmatic sulfide deposits unless large amounts of reducing agents such as organic matter in sediments are assimilated. In contrast, tholeiitic magma produced by decompression melting of mantle is generally more reduced and does not require external reducing materials to stabilize sulfide in the system.

The third model is magmatism associated with lithospheric delamination and asthenosphere upwelling. In applying this model to the Baishiquan and Xiangshan mafic–ultramafic intrusions in the Tianshan region, Chai et al. (2008) adapted a popular view of post-orogenic setting for Permian magmatism in the region whereas B.F. Han et al. (2010) suggested that such event took place during oceanic subduction. Most recently, Li et al. (2011) made some modification based on new data from the Kalatongke sulfide-bearing mafic intrusion in the Chinese Altay (see Fig. 2 for location). They suggested that

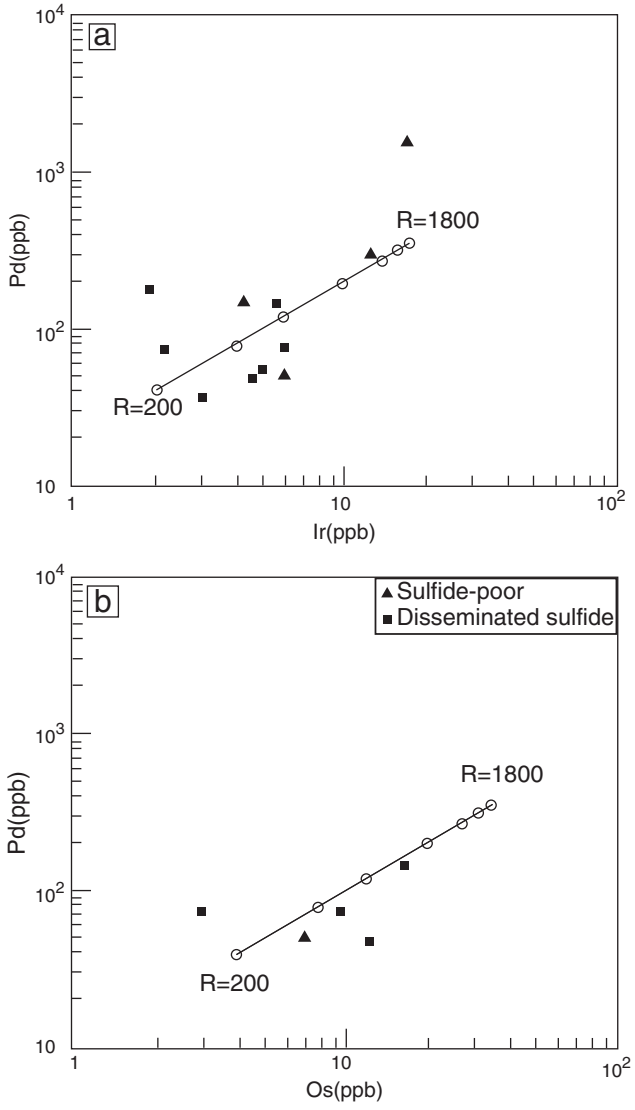

Fig. 12. Plots of Pd versus Ir (a) and Pd versus Os (b) in recalculated 100% sulfide of sulfide-poor and selected disseminated sulfide samples from the Tianyu intrusion. R-factors are magma/sulfide mass ratios calculated using the equation of Campbell and Naldrett (1979). In our calculations the partition coefficients between sulfide melt and coexisting magma for Pd, Ir and Os are assumed to be 3×10^4, which is within the range of experimental results. PGE variations in the sulfide ores of the Tianyu intrusion can be well reproduced using 0.01 ppb Ir, 0.02 ppb Os and 0.2 ppb Pd in the parental magma.

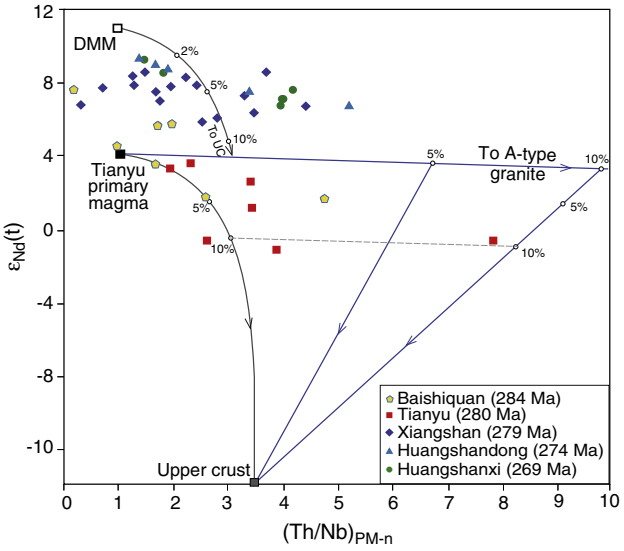

Fig. 13. Plot of ε_{Nd} versus primitive mantle normalized Th/Nb for the Tianyu intrusion and other coeval mafic–ultramafic intrusions in the region. In our mixing calculations the primitive mantle values are from Sun and McDonough (1989); the values for the depleted mantle-derived melt (DMM) represented by N-type MORB are from Zindler and Hart (1986), 0.12 ppm Th, 3.5 ppm Nb, 7.3 ppm Nd, ε_{Nd} (t) = 10.14; the values for the upper crust (UC) are from Rudnick and Gao (2003), 10.5 ppm Th, 12 ppm Nb, 27 ppm Nd, ε_{Nd} (t) = −10; the Tianyu primary magma is assumed to have ε_{Nd} (t) = 4 and Nd, Th, Nb concentrations the same as in the DMM; the values for the coeval A-type granite in the region are from Wang et al. (2009), 36 ppm Nd, 15 ppm Th and 7 ppm Nb (their sample X-387), ε_{Nd} (t) = 3.06 (their sample X-604).

Permian magmatism in the Kalatongke region took place during the transition from oceanic subduction to arc–arc or arc–continent collision. Slab break-off at this stage allowed the underlying oceanic asthenosphere to ascend, thereby triggering decompression melting in the upwelling asthenosphere (Song and Li, 2009; Zhang et al., 2009) to form mafic magma. According to this model, the coeval A-type granites were generated by partial melting in the lower parts of a juvenile arc crust as a result of mafic magma underplating. The parental magma of the Kalatongke mafic intrusion is thought to have formed by mixing of the mantle-derived mafic magma with a small amount of initial melt from the lower arc crust followed by minor contamination with the upper crust (Song and Li, 2009). With reasonable adjustments for the end member compositions and the degrees of crustal contamination, the model of Li et al. (2011) for the Kalatongke intrusion can be used to explain the variations of Sr–Nd isotopes and trace elements in the Tianyu intrusion (Fig. 13).

It is perhaps useful to note that the above competing models have different implications for the evolution of the Tianshan suture zone. A single plume model for basaltic magmatism on both sides of the Tianshan suture implies that the ocean between them was completely consumed by subduction prior to ~290 Ma. The second model suggests that oceanic subduction continued until ~260 Ma. The third model suggests that between ~290 Ma and ~260 Ma the Tianshan region went through a transition from oceanic subduction to arc–arc or arc–continent collision. Age dating of samples from the Tianshan suture zone provides contradictory evidence. The Ar–Ar ages of white mica from retrograde blueschist- and greenschist-facies meta-sediments in the western part of the Tianshan suture are ~320–330 Ma (Wang et al., 2010; and references therein). Different groups have reported different U–Pb ages for overgrown zircon rims in eclogites at different locations in the western part of the Tianshan suture. Zhang et al. (2007) obtained ~230 Ma for the overgrown zircon rims using the SHRIMP method. In contrast, Su et al. (2010) obtained ~320 Ma for the same type of overgrown zircon rims using the SIMS technique.

7. Conclusions

Zircon U–Pb dating reveals that the Tianyu mafic–ultramafic intrusion formed at 280 ± 2 Ma, within the range of many other mafic–ultramafic intrusions in the Tianshan region. The Sr–Nd–Hf isotopes and trace elements of the intrusion are consistent with the model of Permian magmatism due to slab break-off during arc–arc or arc–continent collision. Elevated γ_{Os} values coupled by low PGE tenors in the bulk sulfide ores of the intrusion can be explained by two-stage crustal contamination and associated sulfide segregation. We propose that the first stage took place in the lower part of a juvenile arc crust during mafic magma underplating, and that the second stage occurred when the magma had reached the upper crust. We suggest that the negative Pt anomaly in some semi-massive and massive sulfide ores in the Tianyu intrusion is due to postmagmatic hydrothermal alteration.

Acknowledgments

We are grateful to Song-Lin Cheng, Gang Deng, Jun Li and Xin-Li Zhang for their logistic support for field work, and to Zhong-Li Tang, Bing-Guang Liu, Zhuang-Zhi Qian, Chang-Yi Jiang, and Guang-Ming Li for their advice on regional geology and metalogeny. We thank Prof. E.M. Ripley for his advice on the interpretation of Re–Os isotopes. Constructive reviews from Dr. X-Y Song and anonymous reviewers are appreciated. This study was financially supported by several research grants: the Nature Science Foundation of China (grant 41002026 and 41030424), CAS Knowledge Innovation Project (KZCX2-Y-107), and the CAS Knowledge Innovation Program for Youth Talents to D-M Tang.

References

Amelin, Y., Lee, D.C., Halliday, A.N., Pidgeon, R.T., 1999. Nature of the earth's earliest crust from hafnium isotopes in single detrital zircons. Nature 399, 252–255.
Anders, E., Grevesse, N., 1989. Abundances of the elements: meteoritic and solar. Geochimica et Cosmochimica Acta 53, 197–214.
Ao, S.J., Xiao, W.J., Han, C.M., Mao, Q.G., Zhang, J.E., 2010. Geochronology and geochemistry of Early Permian mafic–ultramafic complexes in the Beishan area, Xinjiang, NW China: implications for late Paleozoic tectonic evolution of the southern Altaids. Gondwana Research 18, 466–478.
Barnes, S.J., Lightfoot, P.C., 2005. Formation of magmatic nickel sulfide ore deposits and processes affecting their copper and platinum group element contents. In: Hedenquist, J.W., Thompson, J.F.H., Goldfarb, R.J., Richards, J.P. (Eds.), Economic Geology 100th Anniversary Volume, pp. 179–213.
Barnes, S.J., Maier, W.D., 1999. The fractionation of Ni, Cu, and the noble metals in silicate and sulphide liquids. Geological Association of Canada Short Course Notes 13, 69–106.
Blichert, T.J., Albarede, F., 1997. The Lu-Hf geochemistry of the chondrites and the evolution of the mantle-crust system. Earth and Planetary Science Letters 148, 243–258.
Campbell, I.H., Naldrett, A.J., 1979. The influence of silicate: sulfide ratios on the geochemistry of magmatic sulfides. Economic Geology 74, 1503–1505.
Chai, F.M., Zhang, Z.C., Mao, J.W., Dong, L.H., Zhang, Z.H., Wu, H., 2008. Geology, petrology and geochemistry of the Baishiquan Ni–Cu–bearing mafic–ultramafic intrusions in Xinjiang, NW China: implications for tectonics and genesis of ores. Journal of Asian Earth Sciences 32, 218–235.
Chen, H.L., Yang, S.F., Dong, C.W., 1997. The discovery of early Permian basic rock belt in the Tarim basin and its tectonic meaning. Geochemica 26, 77–87 (in Chinese).
Fan, W., Zhang, C., Wang, Y., Guo, F., Peng, T., 2008. Geochronology and geochemistry of Permian basalts in western Guangxi Province, Southwest China: evidence for plume–lithosphere interaction. Lithos 102, 218–236.
Gao, J., He, G.Q., Li, M.S., Xiao, X.C., Tang, Y.Q., Wang, J., Zhao, M., 1995. The mineralogy, petrology, metamorphic PTDt trajectory and exhumation mechanism of blueschists, South Tianshan, northwestern China. Tectonophysics 250, 151–168.
Gao, J., Long, L.L., Klemd, R., Qian, Q., Liu, D.Y., Xiong, X.M., Su, W., Liu, W., Wang, Y.T., Yang, F.Q., 2009. Tectonic evolution of the South Tianshan orogen and adjacent regions, NW China: geochemical and age constraints of granitoid rocks. International Journal of Earth Sciences 98, 1221–1238.
Gu, L.X., Chu, O., Hu, S.X., Yan, Z.F., 1990. Geological features and origin of the Kelameili–Harlike alkali granite belt, Xinjiang Province. In: The Editorial Committee of Geoscience of Xinjiang of Project 305 (Eds.). Geoscience of Xinjiang. Geological Publishing House, Beijing, pp. 47–55 (in Chinese with English abstract).
Gu, L.X., Hu, S.X., Chu, Q., Yu, C.S., Xiao, X.J., 1999. Pre-collision granites and post-collision intrusive assemblage of the Kelameili–Harlik orogenic belt. Acta Geologica Sinica 73, 316–329 (in Chinese with English abstract).
Gu, L.X., Zhang, Z.Z., Wu, C.Z., Wang, Y.X., Tang, J.H., Wang, C.S., 2006. Some problems on granites and vertical growth of the continental crust in the eastern Tianshan Mountains, NW China. Acta Petrologica Sinica 22, 1103–1120 (in Chinese with English abstract).
Han, B.F., Wang, S.G., Jahn, B.M., Hong, D.W., Kagami, H., Sun, Y.L., 1997. Depleted-mantle source for the Ulungur River A-type granites from North Xinjiang, China: geochemistry and Nd–Sr isotopic evidence, and implications for Phanerozoic crustal growth. Chemical Geology 138, 135–159.
Han, B.F., Ji, J.Q., Song, B., Chen, L.H., Li, Z.H., 2004. SHRIMP zircon U–Pb ages of Karatongke No.1 and Huangshandong Cu–Ni-bearing mafic–ultramafic complexes, North Xinjiang, and geological implications. Chinese Science Bulletin 49, 2424–2429.
Han, B.F., Guo, Z.J., Zhang, Z.C., Zhang, L., Chen, J.F., Song, B., 2010. Age, geochemistry, and tectonic implications of a late Paleozoic stitching pluton in the North Tian Shan suture zone, western China. GSA Bulletin 122, 627–640.
Han, C.M., Xiao, W.J., Zhao, G.C., Ao, S.J., Zhang, J., Qu, W.J., Du, A.D., 2010. In situ U–Pb, Hf and Re–Os isotopic analyses of the Xiangshan Ni–Cu–Co deposit in Eastern Tianshan (Xinjiang), Central Asia Orogenic Belt: constraints on the timing and genesis of the mineralization. Lithos 120, 547–562.
He, G.Q., Liu, D.Q., Li, M.S., Tang, Y.L., Zhou, R.H., 1996. The five-stage model of crust evolution and metallogenic series of chief orogenic belts in Xinjiang. Xinjiang Geology 13, 100–194 (in Chinese with English abstract).
Hong, D.W., Wang, S.G., Xie, X.L., Zhang, J.S., Wang, T., 2003. Metallogenic province derived from mantle sources: Nd, Sr, S and Pb isotope evidence from the Central Asian orogenic belt. Gondwana Research 6, 711–728.
Hu, A.Q., Jahn, B., Zhang, G.X., Chen, Y.B., Zhang, Q.F., 2000. Crustal evolution and Phanerozoic crustal growth in northern Xinjiang: Nd isotopic evidence. Part I. Isotopic characterization of basement rocks. Tectonophysics 328, 15–51.
Jahn, B.M., 2004. The Central Asia Orogenic Belt and growth of the continental crust in the Phanerozoic. In: Malpas, J., Fletcher, C.J.N., Ali, J.R., Aitchison, J.C. (Eds.), Aspects of the tectonic evolution of China: Geol Soc Lond Spec Publ, 226, pp. 73–100.
Jahn, B.M., Wu, F., Chen, B., 2000. Granitoids of the Central Asian orogenic belt and continental growth in the Phanerozoic. Research of Society Edinburgh: Earth Science 91, 181–193.
Jahn, B.M., Windley, B., Natal'in, B., Dobretsov, N., 2004. Phanerozoic continental growth in Central Asia. Journal of Asian Earth Sciences 23, 599–603.
Jiang, C.Y., Cheng, S.L., Ye, S.F., Xia, M.Z., Jiang, H.B., Dai, Y.C., 2006. Lithogeochemistry and petrogenesis of Zhongposhanbei mafic rock body at Beishan region, Xinjiang. Acta Petrologica Sinica 22, 115–126 (in Chinese with English abstract).
Kamo, S.L., Czamanske, G.K., Amelin, Y., Fedorenko, V.A., Davis, D.W., Trofimov, V.R., 2003. Rapid eruption of Siberian flood-volcanic rocks and evidence for coincidence with the Permian–Triassic boundary and mass extinction at 251 Ma. Earth and Planetary Science Letters 214, 75–91.

Lambert, D.D., Foster, J.G., Frick, L.R., Li, C., Naldrett, A.J., 1999. Re–Os isotopic systematics of the Voisey's Bay Ni–Cu–Co magmatic ore system, Labrador, Canada. Lithos 47, 69–88.
Li, J.Y., 2004. Late Neoproterozoic and Paleozoic tectonic framework and evolution of eastern Xinjiang, NW China. Geological Review 50, 304–322 (in Chinese with English abstract).
Li, C.S., Barnes, S.J., Makovicky, E., Rose-Hansen, J., Makovicky, M., 1996. Partitioning of nickel, copper, iridium, rhodium, platinum and palladium between monosulfide solid solution and sulfide liquid: effects of composition and temperature. Geochimica et Cosmochimica Acta 60, 1231–1238.
Li, J.Y., Wang, K.Z., Li, W.Q., Guo, H.C., Song, B., Wang, Y., Mo, S.G., Zhao, Z.R., Zhu, Z.X., Pan, C.Z., 2003. Tectonic evlution since the late Paleozoic and mineral prospecting in eastern Tianshan Mountains, NW China. Xinjiang Geology 20, 295–301 (in Chinese with English abstract).
Li, H.Q., Chen, F.W., Mei, Y.P., Wu, H., Cheng, S.L., Yang, J.Q., Dai, Y.C., 2006. Dating of the No.1 intrusion of Pobei basic–ultrabasic rocks belt, Xinjiang, and its geological significance. Mineral Deposits 25, 463–469 (in Chinese).
Li, J.Y., Song, B., Wang, K.Z., Li, Y.P., Sun, G.H., Qi, D.Y., 2006a. Permian mafic–ultramafic complexes on the southern margin of the Tu–Ha Basin, east Tianshan Mountains: geological records of vertical crustal growth in central Asia. Acta Geoscientica Sinica 27, 424–446 (in Chinese with English abstract).
Li, J.Y., Wang, K.Z., Sun, G.H., Mo, S.G., Li, W.Q., Yang, T.N., Gao, L.M., 2006b. Paleozoic active margin slices in the southern Turfan–Hami basin: geological records of subduction of the Paleo-Asian Ocean plate in central Asian regions. Acta Petrologica Sinica 22, 1087–1102 (in Chinese with English abstract).
Li, X.H., Liu, Y., Li, Q.L., Guo, C.H., Chamberlain, K.R., 2009. Precise determination of Phanerozoic zircon Pb/Pb age by multi-collector SIMS without external standardization. Geochemistry, Geophysics, Geosystems 10, Q04010. doi:10.1029/cGC002400.
Li, C., Zhang, M., Fu, P., Qian, Z., Hu, P., Ripley, E.M., 2011. The Kalatongke magmatic Ni–Cu deposits in the Central Asian Orogenic Belt, NW China: product of slab window magmatism? Mineralium Deposita. doi:10.1007/s00126-011-0354-7.
Lightfoot, P.C., Keays, R.R., 2005. Siderophile and chalcophile metal variations in flood blasts from the Siberian trap, Noril'sk region: implications for the origin of the Ni–Cu–PGE sulfide ores. Economic Geology 100, 439–462.
Ma, R.S., Wang, C.Y., Ye, S.F., Liu, G.B., 1993. Tectonic Framework and Crustal Evolution of the Eastern Tianshan. Nanjing University Press. (in Chinese).
Mao, J.W., Pirajno, F., Zhang, Z.H., Chai, F.M., Wu, H., Chen, S.P., Cheng, S.L., Yang, J.M., Zhang, C.Q., 2008. A review of the Cu–Ni sulfide deposits in the Chinese Tianshan and Altay orogens (Xinjiang Autonomous Region, NW China): principal characteristics and ore-forming processes. Journal of Asian Earth Sciences 32, 184–203.
Pearce, A., Baker, P.E., Heavy, P.K., Luff, A.W., 1995. Geochemical evidence for subduction fluxes, mantle melting and fractional crystallization beneath the South Sandwich Island Arc. Journal of Petrology 36, 1073–1109.
Pirajno, F., Mao, J.W., Zhang, Z.C., Zhang, Z.H., Chai, F.M., 2008. The association of mafic–ultramafic intrusions and A-type magmatism in the Tian Shan and Altay orogens, NW China: implications for gedodynamic evolution and potential for the discovery of new ore deposits. Asian Journal of Earth Sciences 32, 165–183.
Qi, L., Zhou, M.F., 2008. Platinum-group elemental and Sr–Nd–Os isotopic geochemistry of Permian Emeishan flood basalts in Guizhou Province, SW China. Chemical Geology 248, 83–103.
Qi, L., Zhou, M.F., Wang, C.Y., Sun, M., 2007. An improved Carius tube technique for digesting geological samples in the determination of Re and PGEs. Geochemical Journal 41, 407–414.
Qin, K.Z., 2000. Metallogeneses in relation to Central-Asia type orogeny of Northern Xinjiang. Institute of Geology and Geophysics, Chinese Academy of Sciences, Postdoctoral Research Report. (in Chinese with English abstract).
Qin, K.Z., Zhang, L.C., Xiao, W.J., Xu, X.W., Yan, Z., Mao, J.W., 2003. Overview of major Au, Cu, Ni and Fe deposits and metallogenic evolution of the eastern Tianshan Mountains, Northwestern China. In: Mao, J.W., Goldfarb, R.J., Seltmann, R., Wang, D.W., Xiao, W.J., Hart, C. (Eds.), Tectonic Evolution and Metallogeny of the Chinese Altay and Tianshan (London), pp. 227–249.
Qin, K.Z., Su, B.X., Sakyi, P.A., Tang, D.M., Li, X.H., Sun, H., Xiao, Q.H., Liu, P.P., 2011. SIMS zircon U–Pb geochronology and Sr–Nd isotopes of Ni–Cu–bearing mafic–ultramafic intrusions in eastern Tianshan and Beishan in correlation with flood basalts in Tarim Basin (NW China): constraints on a ca. 280 Ma mantle plume. American Journal of Science 311, 237–260.
Rudnick, R.L., Gao, S., 2003. Composition of the continental crust. In: Rudnick, R.L. (Ed.), Treatise on Geochemistry Volume 3: The Crust. Elsevier, pp. 1–64.
San, J.Z., Qin, K.Z., Tang, D.M., Su, B.X., Sun, H., Xiao, Q.H., Liu, P.P., Cao, M.J., 2010. Precise zircon U–Pb ages of Tulargen large Cu–Ni-ore bearing mafic–ultramafic complex and their geological implications. Acta Petrologica Sinica 26, 3027–3035.
Sengör, A.M.C., Natal'in, B.A., Burtman, V.S., 1993. Evolution of the Altaid tectonic collage and Paleozoic crustal growth in Asia. Nature 364, 299–307.
Shirey, S.B., Walker, R.J., 1998. The Re-Os isotope system in cosmochemistry and high-temperature geochemistry. Annual Review of Earth and Planetary Science 26, 412–500.
Soderlund, U., Patchett, J.P., Vervoort, J.D., Isachsen, C.E., 2004. The Lu-176 decay constant determined by Lu-Hf and U-Pb isotope systematics of Precambrian mafic intrusions. Earth and Planetary Science Letters 219, 311–324.
Song, X.Y., Li, X.R., 2009. Geochemistry of the Kalatongke Ni–Cu–(PGE) sulfide deposit, NW China: implications for the formation of magmatic sulfide mineralization in a postcollisional environment. Mineralium Deposita 44, 303–327.
Song, X.Y., Zhou, M.F., Tao, Y., Xiao, J.F., 2008. Controls on the metal compositions of magmatic sulfide deposits in the Emeishan large igneous province, SW China. Chemical Geology 253, 38–49.
Song, X.Y., Keays, R.R., Zhou, M.F., Qi, L., Ihlenfeld, C., Xiao, J.F., 2009. Siderophile and chalcophile elemental constraints on the origin of the Jinchuan Ni–Cu–(PGE) sulfide deposit, NW China. Geochimica et Cosmochimica Acta 73, 404–424.
Su, W., Gao, J., Klemd, R., Li, J.L., Zhang, X., Li, X.H., Chen, N.S., Zhang, L., 2010. U–Pb zircon geochronology of Tianshan eclogites in NWChina: implication for the collision between the Yili and Tarim blocks of the southwestern Altaids. European Journal of Mineralogy 22, 473–478.
Su, B., Qin, K., Sakyi, P.A., Tang, D., Liu, P., Malaviarachchi, S.P.K., Xiao, Q., Sun, H., 2011. Geochronologic–petrochemical studies of the Hongshishan mafic–ultramafic intrusion, Beishan area, Xinjiang (NW China): petrogenesis and tectonic implications. International Geology Review. doi:10.1080/00206814.2010.543011.
Sun, S.S., McDonough, W.F., 1989. Chemical and isotopic systematics in ocean basalt: implication for mantle composition and processes. In: Saunders, A.D., Norry, M.J. (Eds.), Magmatism in the Ocean Basins: Geological Society of London Special Publications, 42, pp. 313–345.
Tian, W., Campbell, I.H., Allen, C.M., Guan, P., Pan, W., Chen, M., Yu, H., Zhu, W., 2010. The Tarim picrite–basalt–rhyolite suite, a Permian flood basalt from northwest China with contrasting rhyolites produced by fractional crystallization and anatexis. Contributions to Mineralogy and Petrology 160, 407–425.
Wang, J.B., Wang, Y.W., He, Z.J., 2006. Ore deposits as a guide to the tectonic evolution in the East Tianshan mountains, NW China. Geology in China 33, 461–469 (in Chinese with English abstract).
Wang, C.S., Gu, L.X., Zhang, Z.Z., Wu, C.Z., Tang, J.H., Tang, X.Q., 2009. Petrogenesis and geological implications of the Permian high-K calc–alkaline granites in Harlik Mountains of eastern Tianshan, NW China. Acta Petrologica Sinica 25, 1499–1511 (in Chinese with English abstract).
Wang, B., Faure, M., Shu, L., de Jong, K., Charvet, J., Cluzel, D., Jahn, B.M., Chen, Y., Ruffet, G., 2010. Structural and geochronological study of high-pressure metamorphic rocks in the Kekesu section (northwestern China): implications for the late Paleozoic tectonics of the southern Tianshan. Journal of Geology 118, 59–77.
Windley, B.F., Alexeiev, D., Xiao, W.J., Kröner, A., Badarch, G., 2007. Tectonic models for accretion of the Central Asian Orogenic Belt. Journal of the Geological Society of London 164, 31–47.
Wong, K., Sun, M., Zhao, G.C., Yuan, C., Xiao, W.J., 2010. Geochemical and geochronological studies of the Alegedayi Ophiolitic Complex and its implication for the evolution of the Chinese Altai. Gondwana Research 18, 438–454.
Wu, H., Li, H.Q., Mo, X.H., Chen, F.W., Lu, Y.F., Mei, Y.P., Deng, G., 2005. Age of the Baishiquan mafic–ultramafic complex, Hami, Xinjiang and its geological significance. Acta Geologica Sinica 79, 498–502 (in Chinese with English abstract).
Wu, F.Y., Yang, Y.H., Xie, L.W., Yang, J.H., Xu, P., 2006. Hf isotopic compositions of the standard zircons and baddeleyites used in U–Pb geochronology. Chemical Geology 234, 105–126.
Xia, L.Q., Xia, Z.C., Xu, X.Y., Li, X.M., Ma, Z.P., 2008. Petrogenesis of Caboniferous–Early Permian rift-related volcanic rocks in the Tianshan and its neighboring areas, Northwestern China. Northwestern Geology 41, 1–68 (in Chinese with English abstract).
Xiao, W.J., Windley, B.F., Hao, J., Zhai, M.G., 2003. Accretion leading to collision and the Permian Solonker suture, Inner Mongolia, China: termination of the central Asian orogenic belt. Tectonics. doi:10.1029/2002TC001484.
Xiao, W.J., Zhang, L.C., Qin, K.Z., Sun, S., Li, J.L., 2004. Paleozoic accretionary and collisional tectonics of the Eastern Tianshan (China): implications for the continental growth of central Asia. American Journal of Science 304, 370–395.
Xiao, W.J., Windley, B.F., Yuan, C., Sun, M., Han, C.M., Lin, S.F., Chen, H.L., Yan, Q.R., Liu, D.Y., Qin, K.Z., Li, J.L., Sun, S., 2009a. Paleozoic multiple subduction–accretion processes of the southern Altaids. American Journal of Science 309, 221–270.
Xiao, W.J., Windley, F., Huang, B.C., Han, C.M., Yuan, C., Chen, H.L., Sun, M., Sun, S., Li, J.L., 2009b. End-Permian to mid-Triassic termination of the accretionary processes of the southern Altaids: implications for the geodynamic evolution, Phanerozoic continental growth, and metallogeny of Central Asia. International Journal of Earth Sciences 98, 1189–1217.
Xiao, Q.H., Qin, K.Z., Tang, D.M., Sun, B.X., Sun, H., San, J.Z., Cao, M.J., Hui, W.D., 2010. Xiangshanxi composite Cu–Ni–Ti–Fe deposit belongs to comagmatic evolution product: evidence from ore microscopy, zircon U–Pb chronology and petrological geochemistry, Hami, Xinjiang, NW China. Acta Petrologica Sinica 26, 503–522 (in Chinese with English abstract).
Yang, S.H., Zhou, M.F., 2009. Geochemistry of the 430-Ma Jingbulake mafic–ultramafic intrusion in Western Xinjiang, NW China: Implications for subduction related magmatism in the South Tianshan orogenic belt. Lithos 113, 259–273.
Zhang, L.F., Ellis, D.J., Jiang, W., 2002. Ultrahigh pressure metamorphism in western Tianshan, China, part I: evidences from the inclusion of coesite pseudomorphs in garnet and quartz exsolution lamellae in omphacite in eclogites. American Mineralogist 87, 853–860.
Zhang, L.C., Qin, K.Z., Ying, J.F., Xia, B., Shu, J.S., 2004. The relationship between oreforming processes and adakitic rock in Tuwu–Yandong porphyry copper metallogenic belt, eastern Tianshan mountains. Acta Petrologica Sinica 20, 259–268 (in Chinese with English abstract).
Zhang, L.F., Ai, Y.L., Li, X.P., Rubatto, D., Song, B., Williams, S., Song, S.G., Ellis, D.J., Liou, J.G., 2007. Triassic collision of western Tianshan orogenic belt, China: evidence from SHRIMP U–Pb dating of zircon from HP/UHP eclogitic rocks. Lithos 96, 266–280.
Zhang, X.H., Zhang, H., Tang, Y., Wilde, S.A., Hu, Z., 2008. Geochemistry of Permian bimodal volcanic rocks from central Inner Mongolia, North China: implication for tectonic setting and Phanerozoic continental growth in Central Asian Orogenic Belt. Chemical Geology 249, 262–281.
Zhang, Z.C., Mao, J.W., Chai, F.M., Yan, S.H., Chen, B.L., 2009. Geochemistry of the Permian Kalatongke mafic intrusions, northern Xinjiang, Northwest China: implications for the genesis of magmatic Ni–Cu sulfide deposits. Economic Geology 104, 185–203.
Zhang, Y., Liu, J., Guo, Z., 2010a. Permian basaltic rocks in the Tarim basin, NW China: Implications for plume–lithosphere interaction. Gondwana Research 18, 596–610.

Zhang, C.L., Xu, Y.G., Li, Z.X., Wang, H.Y., Ye, H.M., 2010b. Diverse Permian magmatism in the Tarim Block, NW China: genetically linked to the Permian Tarim mantle plume? Lithos 119, 537–552.
Zhang, C.L., Li, Z.X., Li, X.H., Xu, Y.G., Zhou, G., Ye, H.M., 2010c. A Permian large igneous province in Tarim and Central Asian orogenic belt, NW China: results of a ca. 275 Ma mantle plume? GSA Bulletin 122, 2020–2040.
Zhang, M.J., Li, C.S., Fu, P., Hu, P.Q., Ripley, E.M., 2010d. The Permian Huangshanxi Cu-Ni deposit in western China: Intrusive-extrusive association, ore genesis and exploration implications. Mineralium Deposita. doi:10.1007/s00126-010-031803.
Zhou, M.F., Lesher, C.M., Yang, Z.X., Li, J.W., Sun, M., 2004. Geochemistry and petrogenesis of 270 Ma Ni–Cu–(PGE) sulfide-bearing mafic intrusions in the Huangshan district, eastern Xinjiang, northwestern China: implication for the tectonic evolution of the Central Asian Orogenic Belt. Chemical Geology 209, 233–257.
Zhou, D.W., Liu, Y.Q., Xin, X.J., Hao, J.R., Dong, Y.P., Ouyang, Z.J., 2006. Formation of the Permian basalts and implications of geochemical tracing for paleo-tectonic setting and regional tectonic background in the Turpan-Hami and Santanghu basins, Xinjiang. Sciences in China D 49, 584–596 (in Chinese with English abstract).
Zhou, T.F., Yuan, F., Fan, Y., Zhang, D.Y., Cooke, D., Zhao, G.C., 2008. Granites in the Sawuer region of the west Junggar, Xinjiang Province, China: geochronological and geochemical characteristics and their geodynamic significance. Lithos 106, 191–206.
Zhou, M.F., Zhao, J.H., Jiang, C.Y., Gao, J.F., Wang, W., Yang, S.H., 2009. OIB-like, heterogeneous mantle sources of Permian basaltic magmatism in the western Tarim Basin, NW China: implications for a possible Permian large igneous province. Lithos 113, 583–594.
Zhu, X.Q., Wang, Z.G., Wang, Y.L., Bi, H., 2006. Geological characteristics of the post-orogenic alkaline granites in Xinjiang. Acta Petrologica Sinica 22, 2945–2956 (in Chinese with English abstract).
Zindler, A., Hart, S., 1986. Chemical geodynamics. Annual Review of Earth and Planetary Sciences 14, 493–571.